Physics – Uspekhi **58** (12) 1133 – 1158 (2015)

REVIEWS OF TOPICAL PROBLEMS PACS numbers: **12.10.–g**, **12.38.–t**, **12.60–i**, 14.65.Ha

The top quark (20 years after its discovery)

E E Boos, O E Brandt, D S Denisov, S P Denisov, P D Grannis

DOI: 10.3367/UFNe.0185.201512a.1241

Contents

Abstract. This paper, written to mark the twentieth anniversary of the discovery of the top quark, offers some insight into how the understanding of this heaviest known particle has developed from prediction through search to discovery to the current knowledge of its production mechanisms and properties. The central role of the top quark in the Standard Model is considered, and the window of opportunity it opens for seeking new physics beyond the Standard Model is discussed.

E E Boos Skobeltsyn Institute of Nuclear Physics,
Lomonosov Moscow State University,
Leninskie gory 1, str. 2, 119991 Moscow, Russian Federation
E-mail: boos@theory.sinp.msu.ru; Eduard.Boos@cern.ch
O E Brandt Kirchhoff Institute for Physics, Heidelberg University,
69120 Heidelberg, Germany
E-mail: obrandt@kip.uni-heidelberg.de
D S Denisov Fermi National Accelerator Laboratory,
Batavia Illinois 60510, USA
E-mail: denisovd@fnal.gov
S P Denisov Institute for High Energy Physics
of National Research Centre 'Kurchatov Institute',
pl. Nauki 1, 142281 Protvino, Moscow region, Russian Federation
E-mail: denisov@ihep.ru
P D Grannis State University of New York, Stony Brook,
New York 11794, USA
E-mail: pgrannis@sunysb.edu

Received 10 September 2015
Uspekhi Fizicheskikh Nauk **185** (12) 1241 – 1269 (2015)
DOI: 10.3367/UFNr.0185.201512a.1241
Translated by the authors; edited by A Radzig

Keywords: collider, experiment, facility, quark, photon, boson, lepton, hadron, meson, baryon

1. Introduction

Twenty years have passed since the discovery of the heaviest elementary particle, the top quark, in the CDF (Collider Detector at Fermilab) and D0 Tevatron experiments [1, 2]. The top quark, being even heavier than the Higgs boson recently discovered at the Large Hadron Collider (LHC), remains one of the most interesting objects in the elementary particle zoo.

In 1964, Gell-Mann and Zweig [3, 4] developed the quark model to explain the experimental observations in accelerator and cosmic ray experiments of many new strongly interacting particles called hadrons. Originally, it was enough to introduce only three quarks, namely u (up), d (down), and s (strange), to correctly describe the charges and spins of observed hadrons. In this model, all the quarks are spin 1/2 fermions and should have fractional electric charges of $+2/3$ (in units of the electron charge, e) for the u-quark, and $-1/3e$ for the d- and s-quarks. The proton and the neutron are formed from the quark combinations uud and ddu, respectively. The masses of the quarks are a few MeV for u- and d-quarks, and $\sim$100 MeV for the s-quark, based on measured masses of the proton, neutron, π and K mesons, and subsequently on deep inelastic scattering measurements.

In 1974, a new meson called J/ψ was observed [5, 6] which was quickly interpreted as a bound state of a new quark, c (charm), and its antiparticle, with electric charges $\pm 2/3e$. The

charm quark had been predicted theoretically to explain the decay properties of charged and neutral K mesons through the Glashow–Iliopoulos–Maiani (GIM) mechanism [7]. By that time, four electrically and weakly interacting particles [electron (e), electron neutrino (ν_e), muon (μ), and muon neutrino (ν_μ)] were also known, and an interesting symmetric picture appeared containing four quarks, combined into two generations, (u, d) and (c, s), and four leptons similarly arrayed in the corresponding (ν_e, e) and (ν_μ, μ) generations.

In the mid-1970s, this symmetry was broken when the τ lepton was discovered [8] and a new quark, b (bottom), with a mass of about 5 GeV and electric charge of $-1/3e$, was added to the quark family. The b-quark was inferred from the discovery of the Υ-meson at Fermilab [9] with a mass of about 10 GeV, which was seen to be a bound state of b- and $\bar{\text{b}}$-quarks. Subsequent measurements at Cornell, DESY, and SLAC confirmed this interpretation. Assuming that the new lepton and quark belonged to a third fermion generation, then to recover the quark–lepton symmetry the theory needed one more quark and one more neutrino to exist.

The new 'top' quark was discovered in 1995, and in 2000 the tau neutrino was observed in τ-lepton decays in the Fermilab DONUT (Direct Observation of the NU Tau) experiment.

In the Standard Model (SM), the top quark has the same quantum numbers and interactions as all other up type quarks. It is the weak isospin partner of the b-quark with spin 1/2 and electric charge $Q_{\text{em}}^T = +2/3e$. The left chiral part of the top quark is the upper component of the weak isospin doublet, while the right chiral component is a weak isospin singlet. It is a color triplet with respect to the $\text{SU}(3)_\text{c}$ gauge group responsible for the strong interactions in the SM. From the theory side, the top quark is absolutely needed to ensure cancellation of the chiral anomaly in the SM and, therefore, to ensure its consistency as a quantum field theory.

The measured value of the top-quark mass at the Tevatron and the LHC is now known with a precision better than 0.5% and is the most precisely determined mass of a quark: $m_\text{t} = 173.34 \pm 0.27(\text{stat}) \pm 0.71(\text{syst})$ GeV [10].

It is the heaviest known elementary particle, with a mass slightly less than that of the gold nucleus and thus does not conform to the original quark conjecture as a simple constituent of hadrons. However, up to now, we have had no indication of any internal top-quark structure; it behaves in all processes like a pointlike particle.

Two empirical facts distinguish the top from other quarks: its much larger mass, and its very small mixing with quarks of the first and second generations. The natural question arises: Why is the top quark so special? Why is it alone in having a mass of approximately the electroweak (EW) symmetry breaking scale? In the SM there is no answer to this question. In another respect, the top quark is a unique object. The quark mixing in the SM is encoded in matrix elements of the Cabibbo–Kobayashi–Maskawa (CKM) matrix [11, 12]. The matrix element V_tb is close to unity, while the elements V_ts and V_td are significantly smaller than unity. These two experimental facts, large mass and small mixing, lead to the conclusion that in the SM the top quark decays to a W-boson and b-quark with a probability close to 100%.

The width of the top is computed in the SM to be about 1.5 GeV [13, 14], much smaller than its mass. On the other hand, the top width is significantly larger than the typical quantum chromodynamics (QCD) scale $\Lambda \approx 200$ MeV. As a result, the top lifetime ($\tau_\text{t} \approx 5 \times 10^{-25}$ s) is much smaller than the typical time for the formation of QCD bound-state hadrons ($\tau_\text{QCD} \approx 1/\Lambda_\text{QCD} \approx 3 \times 10^{-24}$ s). Therefore, the top quark decays long before it can hadronize and, hence, hadrons containing a top quark are not expected to exist [15]. In this respect, the physics of the top quark is much simpler than, for example, the physics of B-hadrons, in which bound states of the b-quark with other quarks and antiquarks form a rich spectroscopy. However, since the top quark decays before hadronization, its properties are not hidden by hadronization effects and, therefore, it provides a very clean source for fundamental information. In particular, the SM predicts very specific spin correlation properties. Due to the vector–axial vector (V – A) structure of the charged currents in the SM, the top and antitop spins are strongly correlated in production and represent a unique experimental probe in the quark sector through the directions of their decay products.

Two classes of top-quark production exist. The first proceeds by the strong QCD force in which a quark and an antiquark or a pair of gluons interact to produce a top and antitop quark. Since each of the produced tops decays to a W-boson and a b-quark, the final states are determined by the ways that the W-bosons decay. The quarks hadronize in the detector as collimated sprays of hadrons called jets. If both W-bosons decay to charged leptons and neutrinos (*ll* channel), the final state has two leptons, two (b) jets, and missing transverse energy $\not{E}_\text{T}$ carried away by the two neutrinos. If one W decays to a lepton and the other to quark pairs (l + jets channel), the final state comprises one lepton, four jets (of which two are b-jets) and $\not{E}_\text{T}$. If both W-bosons decay to quarks (all-jets channel), the final state has six quark jets. The second production class proceeds through the weak interaction with a W-boson propagator, leading to a single top quark in the final state, associated with at least one other jet.

The top quark, with its large mass and correspondingly large Yukawa coupling $y_\text{t} = 2^{3/4} G_\text{F}^{1/2} m_\text{t} = \sqrt{2} m_\text{t}/v$ (where G_F is the Fermi constant, and v is the vacuum expectation value of the Higgs field) close to unity, makes a significant impact on various electroweak observables due to SM quantum loop corrections involving the top. In particular, the loop corrections to W- and Z-boson masses are proportional to the top mass squared. The fit of precision electroweak data obtained at the Large Electron Positron (LEP) collider experiments and the SLAC Large Detector (SLD) experiment by SM computations at a loop level allowed the indirect estimate of the top-quark mass $m_\text{t} = 177^{+7+17}_{-8-19}$ GeV [16], which was in good agreement with the measurements. A modern global fit of precision electroweak measurements by quantum-loop-corrected SM predictions with a significant top-quark input shows how perfectly the SM works as a quantum gauge theory [17].

The loop contribution involving top quarks is one of the most important factors in the Higgs boson self-coupling evolution with energy scale. It is crucial to know the top-quark mass value precisely to understand how stable the SM vacuum is. The current precision of slightly less than 0.5% does not seem good enough yet to get a concrete answer [18].

Due to the large top-quark mass, the Higgs boson mass parameter also gets large loop corrections which depend quadratically on the scale of possible new physics. Such a dependence may lead to the so-called 'little hierarchy problem' and motivate the possible existence of top-quark

partners which might be accessible at the LHC. Such partners, if they exist, could make extra loop contributions, thus canceling the strong quadratic behavior and stabilizing the Higgs mass parameter.

In the following sections, we discuss various aspects of the top quark in more detail. In Section 2, the history of searches for the top quark at CERN, DESY, and KEK is traced. The top quark's discovery at the Fermilab Tevatron is described in Section 3. In Section 4, we present the measurements of the top pair production cross section. In Section 5, we continue with the discovery of single top production and measurements of the electroweak single top cross section. Due to the importance of the top-quark mass, its measurement and related problems are discussed in a special Section 6. In Section 7, top quark properties such as spin, charge, lifetime, and the CKM matrix element V_{tb} are presented. The special role of the top quark in the SM, particularly in assuring the consistency of the Higgs mechanism of spontaneous electroweak symmetry breaking in the SM, is discussed in Section 8. In Section 9, the role of the top quark as a possible guide to new physics is reviewed. A short conclusion is given in the final section.

2. History of searches for the top quark

The quark model discussed in the previous section (see Fig. 1) and the development of the Standard Model in the 1970s [19–21] implied the existence of a top quark, the charge $+2/3e$ partner of the bottom quark. The search for this new quark went on for twenty years. Using the ratios of the already observed quark masses, some physicists suggested that the top quark might be about three times as heavy as the b-quark, and thus expected that the top would appear as a heavy new meson containing a $t\bar{t}$ pair, with a mass of around 30 GeV.

The electron–positron (e^-e^+) colliders then under construction raced to capture the prize. By 1984, the PETRA e^-e^+ collider at the Deutsches Elektronen-Synchrotron (DESY) in Germany reached a center-of-mass energy of 46.8 GeV and excluded the existence of the top quark with a mass of about half the total center-of-mass energy or 23.3 GeV [22–24]. The e^+e^- collider TRISTAN with an energy of 61.4 GeV was built at the High Energy Accelerator Research Organization (KEK) in Japan in 1986 with the main goal of discovering the top quark. By 1990, experiments at TRISTAN excluded the top quark with a mass of less than 30.2 GeV [25]. Later on, the two e^+e^- Z-boson factories, SLC at SLAC and LEP at CERN, started operation, and by about 1990 set a lower limit on m_t at half of the Z-boson mass: $m_t \geqslant 45.8$ GeV [26–29].

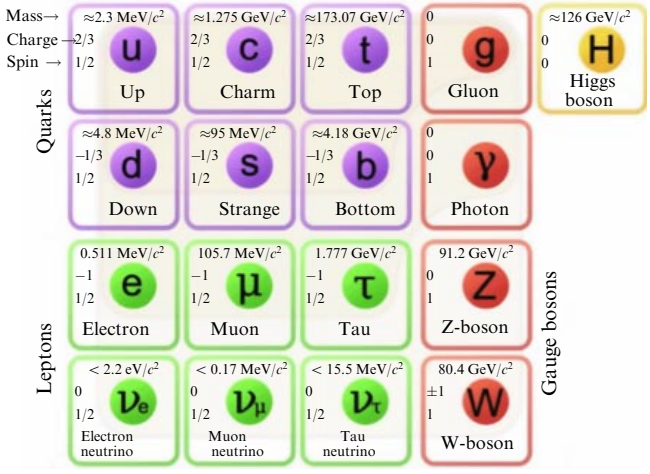

Figure 1. Standard Model table of elementary particles. Similar to the Periodic Table (with substantially more elements), all currently known composite particles are made of quarks and leptons interacting with forces exchanged by the gauge bosons. Each particle has an antiparticle with the same mass and spin, but opposite electric charge. All of the above particles have no observed substructure down to distances of 10^{-18} cm. The Higgs boson supplies mass to most elementary particles.

In the early 1980s, the Super Proton–Antiproton Synchrotron (Sp$\bar{p}$S) collider came into operation at CERN with counter-rotating beams of protons and antiprotons colliding with an energy of 540 GeV (later upgraded to 630 GeV). The protons and antiprotons brought their constituent quarks and antiquarks into collisions with typical energies of 50 to 100 GeV. Besides the important discoveries of the W- and Z-bosons which are the carriers of the unified electroweak force, the CERN experiments demonstrated another aspect of quark behavior. Though quarks had continued to elude direct detection, they can be violently scattered in high-energy collisions. The high-energy quarks emerging in the collision region are subject to the strong interaction, creating additional quark–antiquark pairs from the available collision energy. The quarks and antiquarks so created combine into ordinary hadrons that are observed at the detectors. These hadrons tend to cluster along the direction of the original quark, and are thus recorded as a 'jet' of rather collinear particles. Such quark jets, previously sensed at SLAC and DESY, were clearly observed at CERN and became a key ingredient in the next round of top quark searches.

With the advent of the Sp$\bar{p}$S, and the more powerful 1800 GeV Tevatron collider at Fermilab in 1988, the search for the top quark turned to even higher masses. At the large masses now accessible, the $t\bar{t}$ bound state was unlikely to form (as the top quark would decay faster than the time needed for binding the quarks into a bound state), so the decays of isolated top quarks were expected. For $m_t < m_W$, the W-boson decay into a top quark and a b-quark would occur. A good channel for the search was $W^+ \to t\bar{b} \to e^+\nu_e b\bar{b}$ and the charge-conjugate process. The main background would be the QCD production of W-bosons and jets in the strong interactions.

In 1984, the UA1 experiment at the Sp$\bar{p}$S reported evidence of an excess of events with an isolated lepton and two jets, characteristic of a 40-GeV top quark [30]. UA1 observed 6 events (3 with electrons and 3 with muons) with an expected background of less than 1 event. In retrospect, the background from $b\bar{b}$ production was underestimated, and the top quark 'observation' was later ruled out [31, 32].

Table 1. Summary of increasing mass limits on the mass m_t of the top quark through the 1980s and early 1990s.

Year	Collider	Coll. particles	Limit on m_t, ГэВ	References
1984	PETRA (DESY)	e^+e^-	> 23.3	[22–24]
1990	TRISTAN (KEK)	e^+e^-	> 30.2	[25]
1990	SLC (SLAC), LEP (CERN)	e^+e^-	> 45.8	[26–29]
1988	Sp$\bar{p}$S (CERN)	$p\bar{p}$	> 45	[31]
1990	Sp$\bar{p}$S (CERN)	$p\bar{p}$	> 69	[32]
1991	Tevatron (Fermilab)	$p\bar{p}$	> 91	[33]
1994	Tevatron (Fermilab)	$p\bar{p}$	> 131	[34]

3. Top-quark discovery at the Tevatron

In 1988, the search for the top quark was joined by the CDF experiment in the first physics run of the newly commissioned Tevatron $p\bar{p}$ collider [34] operating at 1.8 TeV. Based on the unsuccessful searches for top-quark pairs $t\bar{t}$ at e^-e^+ colliders and those at the CERN Sp$\bar{p}$S seeking top quarks from the decay $W \to t\bar{b}$, it became increasingly likely that the top quark would have a mass greater than the W-boson. By then, the precision measurement of observables in Z-boson decay, neutrino scattering, and the mixing of the neutral K^0 and B^0 flavor eigenstates predicted that the top-quark mass m_t lay most likely in the approximate range $90 < m_t < 160$ GeV, based on analyzing the indirect effects of top-quark loops in these processes within the context of the SM.

In 1992, CDF Collaboration reported a new search for top-quark pair production [33] in which both top quarks decay to a W-boson (real or virtual, depending on the top mass) and a b-quark. The search used the *ll* channel, as well as the $l +$ jets channel. In the latter channel, CDF required at least one of the jets to be tagged as a b-jet, identified through the presence of a low p_T (soft) muon from the semileptonic decay of a B-hadron. Comparison of the observed yield of events with SM predictions as a function of m_t gave a lower limit of 91 GeV, thus ruling out the possibility that the W-boson decays to top quarks and implying that the dominant production mode would be $t\bar{t}$ pair production.

In 1992, the new D0 experiment, with its high-resolution liquid argon calorimeter and large electron and muon acceptances, began operation at the Tevatron, and in 1994 raised the lower limit to 131 GeV [35], now encroaching on the window set indirectly by the precision measurements. For this run, CDF put a new silicon microstrip vertex detector close to the interaction region that permitted the identification of jets containing a b-hadron that travelled a short distance (a few mm) from the production point, providing a powerful tool for recognition of b-quark jets and suppression of background processes due to W + jets and QCD multijet production.

Although both collaborations were still setting lower limits on m_t, the bounds were not much improved as the data samples increased. In the winter of 1992–1993, both collaborations recorded striking events that conformed to the profile expected for top-quark pair events. Both events occurred in the eμ dilepton channel, which had a low background. The CDF event had one of the two jets tagged by its silicon microstrip detector as a b-jet (as well as by a soft muon). The D0 event had an electron, muon, and $\not{E}_T$, each with at least 100 GeV transverse momentum. These events were very unlikely to have arisen from the expected background processes and heightened the expectation of a top-quark discovery.

By early 1994, CDF found more $t\bar{t}$-like events in 19 fb^{-1} of data than were predicted by known backgrounds. Publication [36] claimed evidence of the top-quark production and reported 12 events in the dilepton channel and the $l +$ jets channel with at least one jet tagged as a b-quark jet by the vertex detector or a soft muon within the jet. The probability of the background fluctuating to the observed yield was 0.26%, too large to claim the result as a discovery, but small enough to interpret the excess as being likely to arise from top-quark production. The fitted mass was $m_t = 174 \pm 16$ GeV, and the $t\bar{t}$ cross section was estimated to be approximately 14 pb, a factor of about two larger than expected from theory at the observed m_t value. Shortly afterwards, D0 reported [37] the results of an analysis in which backgrounds were reduced through the use of topological variables that had a comparable expected sensitivity to CDF, but with only 7 observed events and a 7.2% probability of the background explaining the observed yield.

The appearance of events in excess of the background expectation created the anticipation in both collaborations that more data could bring discovery. During a Tevatron shutdown in summer 1994, the accelerator experts discovered that one of the bending magnets in the machine had been mistakenly rotated around the beam axis. With this fixed, the instantaneous collider luminosity grew substantially and, by early 1995, the data samples had approximately tripled relative to the 1994 evidence results, and both collaborations sensed that they were sufficient to permit the discovery. Both collaborations updated their selection criteria to optimize the sensitivity for a top quark with mass in the 150–200 GeV region. Although there were no information exchanges between the collaborations on their progress, each knew that the other was getting close and each began a frenetic push to complete the analyses. An agreement had been put in place that when either collaboration presented a paper draft to the Fermilab director, a one week period would start during which the other collaboration could finalize a paper, and if so, a simultaneous submission for publication would occur. CDF delivered its paper in mid-February and, one week later, on 24 February 1995, both collaborations submitted their discovery papers to *Physical Review Letters*. The results were embargoed until the seminar announcing the results on 2 March, but a few days before, newspaper reporters had picked up the scent and reported on the impending announcement.

In the discovery publications [1, 2], CDF and D0 collaborations presented quite complementary analyses. CDF relied heavily on its b-tagging capability, and claimed a one in a million probability of the expected backgrounds producing the observed yield of 6 dilepton events, 21 $l +$ jet events with a b-quark jet tagged by the vertex detector (with 27 jets tagged), and 22 $l +$ jets events tagged by a muon within the jet (with 23 jets tagged), with an estimated background component of 1.3 dilepton events and 6.7 and 15.4 tagged jets for the two categories of single-lepton events.

D0 used stricter selection cuts based on the topological variables H_T, defined as the sum of the scalar $\not{E}_T$ of the objects in the event, and the aplanarity measuring the tendency for the momenta of the objects to lie in a plane, to suppress backgrounds. D0 found 3 dilepton events, 8 $l +$ jets events with topological cuts, and 6 events with a b-jet tagged with a soft muon, with estimated backgrounds of 0.65, 1.9, and 1.2 events, respectively, for the three categories, with an estimated probability for the background to fluctuate to the observed yields of two in a million. For the $l +$ jets events, a measure of the top mass could be reconstructed from the four-momenta of the observed objects and a fit for the neutrino momentum using the W-mass as a constraint. This fitted mass was then compared with a family of Monte Carlo templates with varied input masses to obtain the most likely top-quark mass.

Figure 2 shows the fitted mass distributions from the discovery papers. CDF reported a mass of $m_t = 176 \pm 13$ GeV, and D0 found $m_t = 199 \pm 30$ GeV. Using the observed yields and accounting for experimental efficiencies and acceptances, the cross section for $t\bar{t}$-pair production

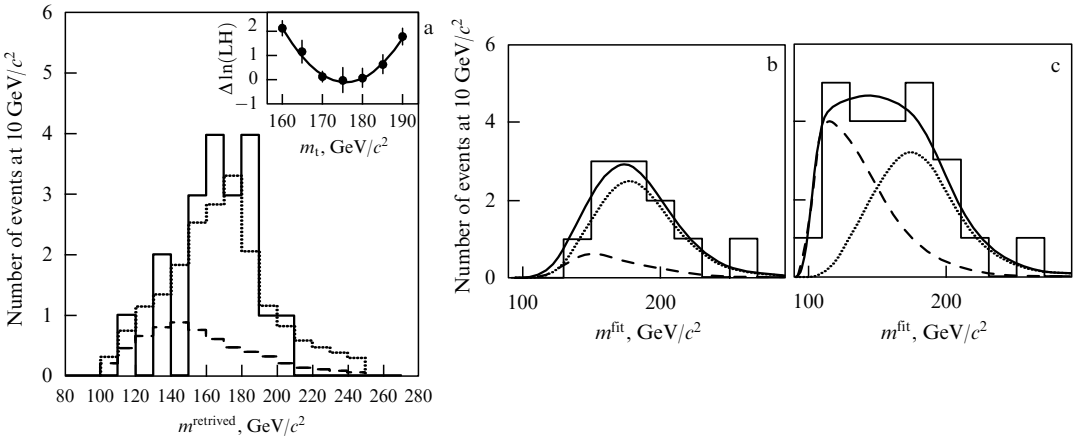

Figure 2. Reconstructed mass distributions of single-lepton candidate events showing the data (solid histogram), expected background, and expected $t\bar{t}$ signal for the CDF (left) and D0 (right) measurements. The CDF panel inset shows the log-likelihood distribution as a function of assumed mass and the fit for the best mass value. The two elements of the D0 panel show the result for (a) the standard analysis, and (b) an analysis with loosened selection criteria.

could be evaluated. CDF found $\sigma_{t\bar{t}} = 6.8^{+3.6}_{-2.4}$ pb, and D0 arrived at $\sigma(t\bar{t}) = 6.4 \pm 2.2$ pb. The results were consistent with each other and with the modern measurements of the mass and cross section. D0 also presented the two-dimensional plot of the mass of two jets (from hadronic W-decay) versus the three jet mass (the hadronic top decay) that supported the hypothesis for the decay $t \to Wb$.

Both collaborations saw an excess of events, whose confidence level was a little lower than a 5σ deviation from a background-only hypothesis, but the joint result had more than 5σ significance and gave rise to the modern standard of requiring 5σ for a discovery.

The strikingly large mass of the observed top quark stimulated the subsequent program of measurements described in the succeeding Sections 4–9.

4. Top-antitop pair production

Up until 2009, the top quark could only be produced at the Tevatron. The 2001–2011 run acquired about 10 fb^{-1} of data using $p\bar{p}$ collisions at 1.96 TeV, or about 200 times that used for the 1995 discovery. In 2009, the LHC came into operation using pp collisions, first at 7 TeV, increasing to 8 TeV in 2012 and then to 13 TeV in 2015. The general purpose ATLAS (A ToroidaL LHC ApparatuS) and CMS (Compact Muon Solenoid) experiments have accumulated large samples of top-quark events, augmented by data from the LHCb (LHC beauty) experiment in some kinematic regions.

The production of $t\bar{t}$ pairs proceeds through the annihilation of a quark (q) and an antiquark ($\bar{q}$) or through interaction of gluons in the colliding beam particles. At the Tevatron $p\bar{p}$ collider, the $q\bar{q}$ processes account for about 85% of the cross section, whereas at the LHC pp collider, the gluon–gluon (gg) process is dominant ($> 80\%$).

Recently, the complete next-to-next-to-leading order (NNLO) QCD calculations of the inclusive $t\bar{t}$-pair production cross sections have been performed [38] with estimated uncertainties of 2.2% (Tevatron) or 3% (LHC) due to higher-order contributions. Some differential cross sections have also been calculated in the NNLO approximation [39]. Precise measurements of inclusive and differential cross sections can thus provide sensitive tests of the SM. Since the top quark decays prior to hadronization, information on the spin correlations and polarizations of t- and $\bar{t}$-quarks can also be obtained from studying the pair production processes.

The Tevatron measurements of the inclusive $t\bar{t}$ cross sections as of 2013 are summarized in Fig. 3a. The combination of CDF and D0 results [40] yields $\sigma_{t\bar{t}} = 7.60 \pm 0.41$ pb, in good agreement with the NNLO theoretical prediction [38] of 7.16 pb. Recent D0 updates of the $l+$jets and dilepton channel cross sections using the full 9.7 fb^{-1} of data are combined to give $\sigma_{t\bar{t}} = 7.73 \pm 0.56$ pb [41]. The individual ATLAS and CMS inclusive cross section measurements at $\sqrt{s} = 8$ TeV and their combined result, $\sigma_{t\bar{t}} = 241.5 \pm 8.5$ pb [42], shown in Fig. 3b, are also in good agreement with the NNLO prediction of 245.8 pb [38]. Cross sections for the forward production of top quarks at 7 and 8 TeV consistent with SM predictions have recently been reported by the LHCb Collaboration [43].

Measurements of differential cross sections offer a more sensitive way to seek new phenomena in the top-quark sector. Many models postulate a special role for the top quark in coupling to new non-SM physics, which could be revealed through resonances observed in the $t\bar{t}$ mass distribution or departures from SM predictions in transverse momentum (p_T) or rapidity (y) distributions. Such distributions have been measured at the Tevatron [44] and more recently at the LHC [45], where the higher collision energy allows a much larger region of $m_{t\bar{t}}$ to be explored. To date, as shown in Fig. 4, departures from SM behavior has not been observed for $m_{t\bar{t}} < 2.5$ TeV.

Possible new physics coupling to the top quark can be sought through the production of heavy objects in association with a $t\bar{t}$ pair, particularly at the LHC, where the available phase space is larger than at the Tevatron. New physics models such as supersymmetry predict such associated production final states, for example, through the production of bottom quark pairs with a decay chain $\tilde{b} \to t\tilde{\chi}_1^-$ and $\tilde{\chi}_1^- \to W^-\tilde{\chi}_1^0$ (and charge conjugate). Other models may enhance the SM cross sections for $t\bar{t}+X$ final states through new couplings (e.g., dimension six operators [46]). ATLAS and CMS have obtained evidence for the production of $t\bar{t}$ pairs with associated b- or c-quarks [47], W- or Z-bosons [48–51], and $b\bar{b}$ [52], and have set limits on $t\bar{t}t\bar{t}$ production [53–55]. All these results are in good agreement with the SM predictions, as shown in Fig. 5.

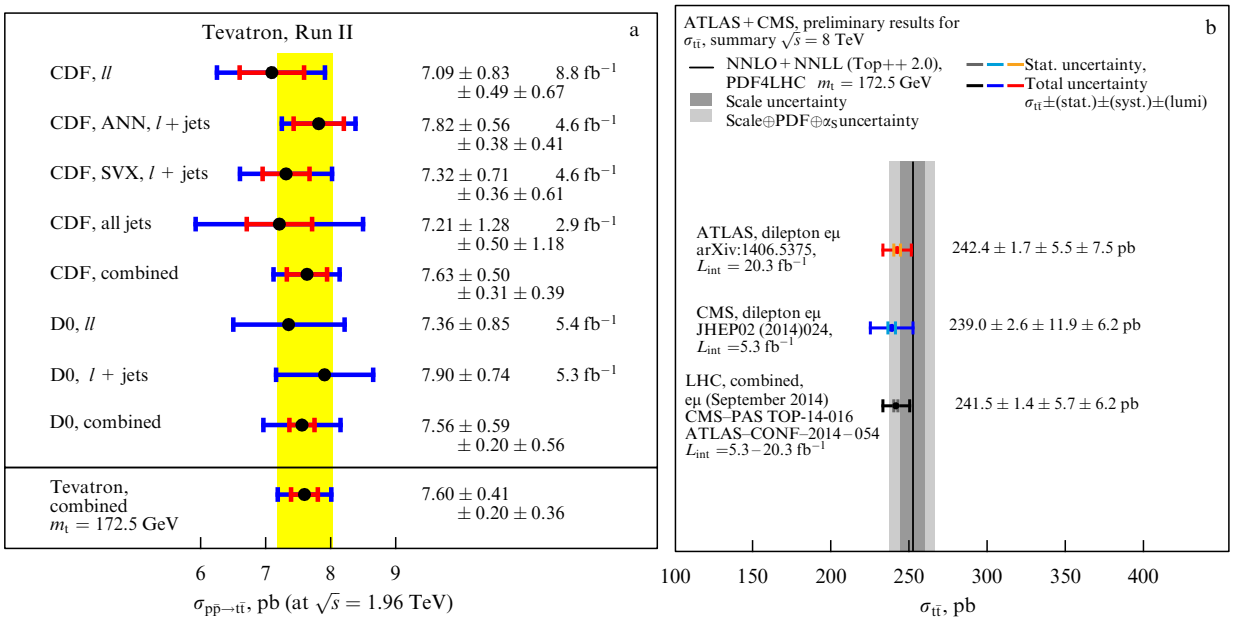

Figure 3. (Color online.) The $t\bar{t}$ inclusive cross section measurements at (a) the Tevatron and their combination; (b) the LHC and their combination.

At the leading order (LO) QCD, the annihilation of valence quarks and antiquarks in $p\bar{p}$ collisions at the Tevatron is not expected to give a preference for the t (or $\bar{t}$) to emerge in the proton hemisphere relative to the antiproton hemisphere. At the next-to-leading-order (NLO), however, interferences between the LO Born and loop diagrams or initial and final state gluon radiation diagrams result in an expected small positive forward–backward asymmetry

$$A_{\rm FB}^{t\bar{t}} = \frac{N(\Delta y > 0) - N(\Delta y < 0)}{N(\Delta y > 0) + N(\Delta y < 0)} ,$$

where $\Delta y = y_t - y_{\bar{t}}$. The 2011 CDF measurement of $A_{\rm FB}^{t\bar{t}}$ in the l + jets channel with 5.3 fb^{-1} of data [56], in which the top quarks were unfolded to the parton level, gave $A_{\rm FB}^{t\bar{t}} = 0.158 \pm 0.074$, somewhat in tension with the then-existing NLO QCD prediction of about 0.06. The measured asymmetry grew with both Δy and $m_{t\bar{t}}$; for $m_{t\bar{t}} > 450$ GeV, the discrepancy with NLO QCD reached 3.4σ. The 2011 D0 lepton + jets measurement [57] yielded $A_{\rm FB}^{t\bar{t}} = 0.092 \pm 0.037$, statistically compatible with both the CDF result and the NLO QCD prediction. These early measurements stimulated much theoretical activity [58] to find potential sources of new physics that could enhance the SM prediction, such as axigluon or Z' production.

By 2014, both the theoretical and experimental situations were clarified. A complete NNLO calculation (thus, next-to-leading order in the asymmetry) found $A_{\rm FB}^{t\bar{t}} = 0.095 \pm 0.007$ [39]. Both CDF and D0 Collaboration published results for the l + jets channel with the full Tevatron data sample [59, 60], with inclusive asymmetry values $A_{\rm FB}^{t\bar{t}} = 0.164 \pm 0.047$ and $A_{\rm FB}^{t\bar{t}} = 0.106 \pm 0.030$, respectively. Figure 6 shows the results as a function of Δy and $m_{t\bar{t}}$ for both experiments and the NNLO predictions.

The $t\bar{t}$ asymmetry in the dilepton channel has also been measured by D0 [61] to be $A_{\rm FB}^{t\bar{t}} = 0.175 \pm 0.063$. A related lepton asymmetry

$$A_{\rm FB}^{l} = \frac{\left(N(q_l\eta_l) > 0\right) - \left(N(q_l\eta_l) < 0\right)}{\left(N(q_l\eta_l) > 0\right) + \left(N(q_l\eta_l) < 0\right)} ,$$

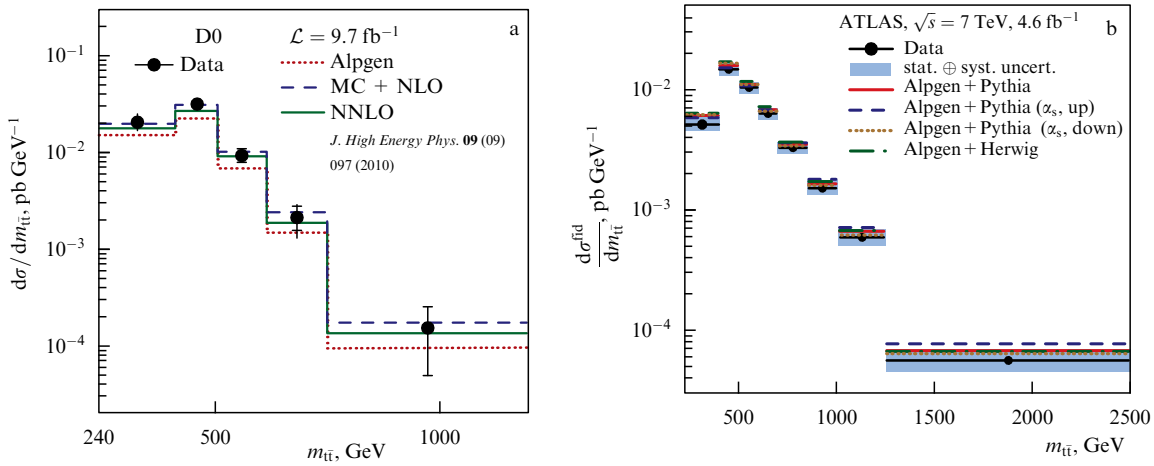

Figure 4. (Color online.) Differential $t\bar{t}$ production cross sections as functions of $m_{t\bar{t}}$ for (a) D0, and (b) ATLAS experiments.

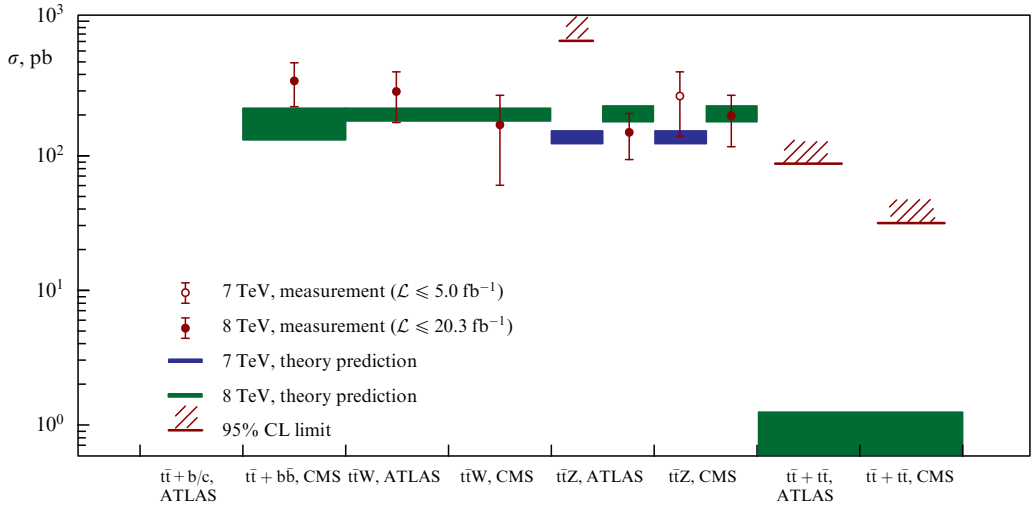

Figure 5. (Color online.) ATLAS and CMS measurements and limits for $t\bar{t}$ production in association with vector bosons and heavy quark pairs.

where q_l is the sign of the lepton electric charge, and η_l is the pseudorapidity of the lepton, has been measured in the combined ll and $l+$jets and dilepton channels with the following results for CDF [62] and D0 [63]: $A_{\rm FB}^{l} = 0.090^{+0.028}_{-0.026}$ and $A_{\rm FB}^{l} = 0.047 \pm 0.027$, respectively, to be compared with the NLO prediction of $A_{\rm FB}^{l} = 0.038 \pm 0.003$ [64]. The asymmetry in the pseudorapidity difference between the two lepton rapidities can only be measured in the dilepton channel and is consistent with NLO QCD in both Tevatron experiments [62, 65].

Overall, the forward–backward asymmetries at the Tevatron have settled down to reasonable agreement with the most accurate predictions of QCD, with CDF results typically exceeding the prediction by roughly 1.5σ, and the D0 results in agreement with QCD to within 1σ.

At the LHC, the pp symmetric initial state does not permit the distinction between forward and backward directions to be made, so a central-forward asymmetry is defined instead:

$$A_{\rm C} = \frac{\big(N(\Delta|y|) > 0\big) - \big(N(\Delta|y|) < 0\big)}{\big(N(\Delta|y|) > 0\big) + \big(N(\Delta|y|) < 0\big)},$$

where $\Delta|y| = |y_t| - |y_{\bar{t}}|$. The NLO prediction for $A_{\rm C}$ is about 1%, making this measurement difficult. Current preliminary measurements made by ATLAS [66, 67] and CMS [68–70] with an accuracy of 1–2% are all consistent with $A_{\rm C} = 0$.

Since the top-quark weak interaction decay is much shorter than the time required for hadronization by the strong interaction, the spin orientations of the resultant top quarks can be sensed through angular distributions of the decay products. Although the polarizations of t or $\bar{t}$ are expected to be close to zero in the SM, the correlation between the spin orientations is expected to be large. For the gg process that is dominant at the LHC, the gluons have mainly the same helicities at low $m_{t\bar{t}}$, and mainly opposite helicities at high $m_{t\bar{t}}$. At the Tevatron, the production of top quarks proceeds mainly from opposite helicities of q and $\bar{q}$ in the initial state, and thus the two colliders provide complementary information. The polar angle distributions of final state fermions in the $t\bar{t}$ rest frame can be written as

$$\frac{1}{\sigma}\frac{{\rm d}\sigma}{{\rm d}\cos\theta_1\cos\theta_2} = \frac{1}{4}\,(1 + \alpha_1 P_1\cos\theta_1 + \alpha_2 P_2\cos\theta_2 + \alpha_1\alpha_2 A\cos\theta_1\cos\theta_2)\,, \qquad (1)$$

where θ_i is the decay fermion polar angle, P_i is the polarization, α_i is the spin-analyzing power for the ith particle, and A is the spin correlation in the $t\bar{t}$ strong production process. The parameters α are near 1 for a charged lepton or down type quarks, and 0.31 for up type quarks. The spin quantization axes are chosen in the scattering plane and therefore may be aligned in the beam

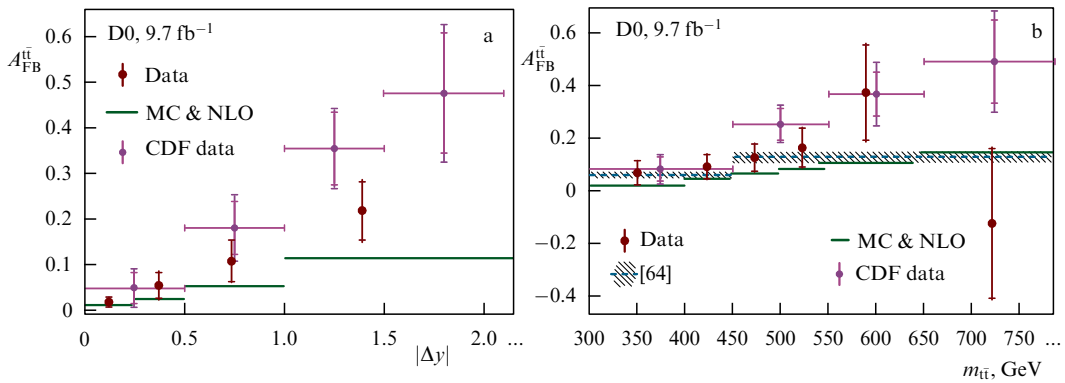

Figure 6. (Color online.) The D0 and CDF measurements of $A_{\rm FB}$ as a function of (a) Δy, and (b) $m_{t\bar{t}}$, compared with the NNLO QCD predictions taking account of NLO electroweak corrections from Ref. [39].

direction, in the outgoing t-quark direction (helicity basis), or along an intermediate axis chosen to achieve maximum expected spin correlation. In the case of top-quark production via the gg process, the distribution as a function of the azimuthal angle difference between decay leptons in dilepton events also carries information on the spin correlation.

D0's measurement of the spin correlation in the beam basis yielded $A = 0.85 \pm 0.29$ using both the lepton + jet and dilepton channels [71]. This result is in good agreement with the SM prediction of $A = 0.78^{+0.03}_{-0.04}$ [72] and departs by 3.1σ from the no-correlation hypothesis ($A = 0$). CDF's measurement [73] in the helicity basis has led to $A = 0.60 \pm 0.22$ that is also in good agreement with QCD. The first observations of a nonzero spin correlation were made by ATLAS [74] and CMS [75] using the azimuthal angle between the two leptons in the dilepton sample in dominantly gg interactions, for both the helicity basis and the intermediate basis. Subsequent addition of the lepton + jet decay channel allowed ATLAS [76] to measure several correlation observables in different bases, which are sensitive to different manifestations of new physics in $t\bar{t}$ pair production.

The top-quark parity-violating polarization in the scattering plane is very close to zero in the SM, so measurable nonzero polarization would signal new physics. The actual extent of polarization depends upon the choice of basis for spin quantization; common choices are the helicity basis (the t-quark momentum direction) or the beam basis (the incoming proton direction), both in the $t\bar{t}$ rest frame.

A D0 determination of the polarization in the beam basis, $\mathcal{P} = 11.3 \pm 9.3\%$, was made in conjunction with the forward–backward asymmetry measurement in the dilepton channel [61]. Preliminary polarization measurements were recently performed by D0 in the l + jets channel in the beam (helicity) basis with the results $P = 7.0 \pm 5.5\%$ ($-10.2 \pm 6.0\%$), as well as the parity-conserving polarization normal to the scattering plane: $P = 4.0 \pm 3.4\%$ [77]. Both ATLAS and CMS experiments have measured polarizations at 7 TeV in the helicity basis. ATLAS determined CP-even and CP odd polarizations of -0.035 ± 0.040 and 0.020 ± 0.022 [78], respectively. CMS found the CP-even polarization to be 0.005 ± 0.021 [75].

Recently, the parity-violating polarization of single top quarks produced by the weak interaction has been measured by CMS to be $P = 0.82 \pm 0.34$ [79], in good agreement with the NLO SM prediction of 0.88.

5. Single top production

Top quarks are mainly produced as $t\bar{t}$ pairs in the strong interaction reactions at hadron colliders. It was in this process that the top quark was discovered at the Tevatron and in which the majority of the top-quark studies were performed. But, as first proposed in Ref. [80], top quarks could also be produced individually in high-energy collisions via the two electroweak processes shown in Fig. 7. A third process in which a top quark is produced in association with the W-boson has a negligible cross section at the Tevatron but becomes important at the LHC, as discussed below. The dominant t-channel process proceeds through the exchange of a spacelike virtual W-boson between a light (u, d, c, s) quark and a b-quark. The subdominant process involves the exchange of a timelike virtual W-boson in the s-channel producing a top quark and a b-quark.

The production cross sections at the Tevatron are predicted to be 1.12 pb (s-channel) and 2.34 pb (t-channel) [81]. Somewhat surprisingly, the total electroweak single top quark cross section is about half of that for the strong interaction $t\bar{t}$-pair production value of 7.16 pb [38]. The main reason lies in the fact that the effective mass of the final state products in individual top production is about half of that for pair production, so that the much more abundant lower-momentum quarks and gluons in the interacting proton and antiproton can give the single top quarks. However, the smaller number of jets and leptons in single top production compared with $t\bar{t}$ production makes individual top-quark detection difficult due to the more copious backgrounds. Thus, about 50 times more luminosity and 14 more years were required to discover electroweak single top quark production after the top quark discovery in $t\bar{t}$ pair production via the strong interaction.

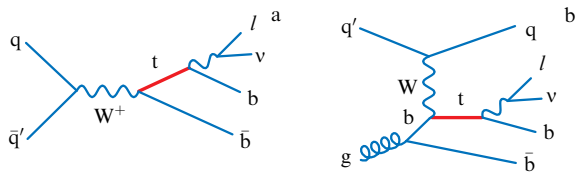

Figure 7. Feynman diagrams of the single top quark production via the (a) s-channel process, and (b) t-channel process.

The observation of single top quark production was reported by the CDF and D0 Collaborations in 2009 using about 3 fb^{-1} of Tevatron data [82, 83]. The high W + jets background, with its larger cross section but similar final event topology (Fig. 7), posed the major challenge. After an initial 'cut based' events selection based on the kinematic parameters of the events, the signal fraction in the analysis sample was only $\approx 5\%$, well below the uncertainty of the background prediction.

The only option for firmly establishing the existence of the single top quark events was the use of multivariate analysis methods [84, 85] which combine tens of event parameters into a single discriminant that provides a good separation of signal and background. This discriminant uses not just the difference in signal and background distributions in each parameter but also the correlations among them. The multivariate classifiers were trained on large Monte Carlo samples of signal and background events. Discriminant distributions are plotted in Fig. 8 for the CDF and D0 discovery analyses in which single top quark events concentrate on the large values of the discriminant.

The discovery of single top quark production not only firmly established that electroweak single top production conforms to the SM prediction, but also verified for the first time that the power of multivariate analyses could be applied for particle physics discoveries. Many subsequent discoveries in particle physics, including that of the Higgs boson, relied heavily on the multivariate methods developed at the Tevatron for observing the single top quark production. These searches also spawned the development of new theoretical tools, such as single top quark event generators [86].

With 10 fb^{-1} per Tevatron experiment accumulated by the end of the Tevatron run, together with improvements in the analysis methods, precise studies of single top quark production became possible, including the independent observation of the single top quark t-channel and s-channel processes and measurement of their cross sections. A combination of CDF

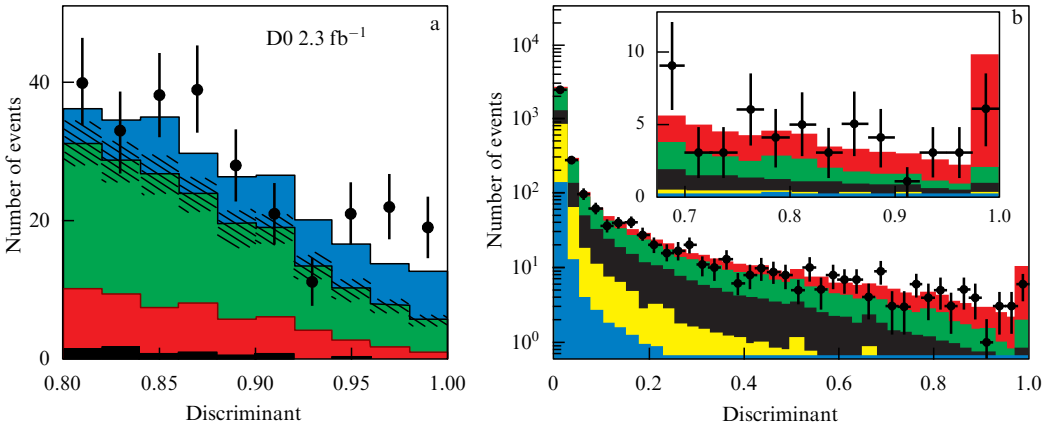

Figure 8. (Color online.) Observation of single top quark production at the Tevatron. The D0 discriminant distribution is represented in figure (a), where the single top quark signal is shown in blue and shaded areas indicate the background uncertainty. The CDF discriminant distribution is plotted in figure (b), indicating an excess of events at the large discriminant values in comparison with background predictions (nonred colors). Red color indicates the single top quark contribution.

and D0 results was required for the 6.3σ observation of the s-channel process [87]. Figure 9 summarizes single top quark production data at the Tevatron based on the full data set. The s- and t-channel cross sections are in agreement with the SM predictions.

The single top quark production cross section is approximately proportional in the SM to the square of the CKM matrix element V_{tb} [11, 12]. By extracting V_{tb} from the measured single top quark cross sections and including uncertainties in the predictions, this parameter may be measured directly without assumptions on the number of quark generations or on the unitarity of the CKM matrix. The Tevatron measurement result for, $V_{tb} = 1.02^{+0.06}_{-0.05}$, shown in Fig. 10, is in agreement with the V_{tb} value obtained with the assumptions of CKM matrix unitarity and three quark generations [88].

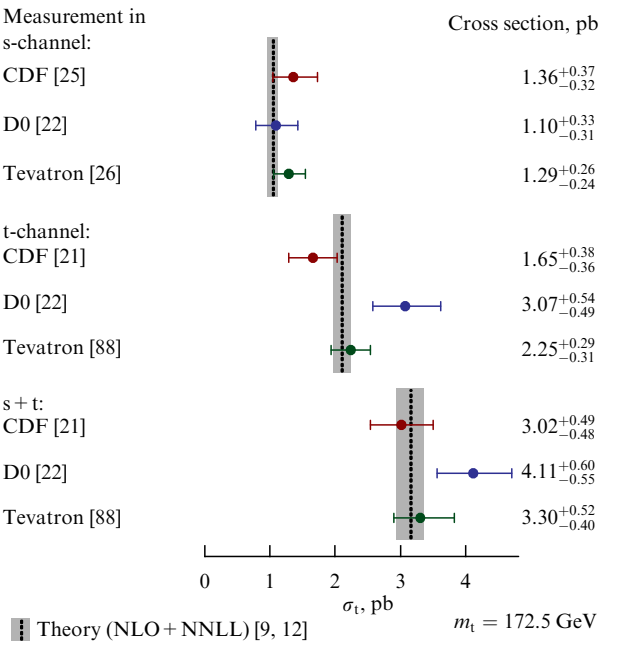

Figure 9. (Color online.) Tevatron single top quark production cross section summary, taken from Ref. [88]. References in the figure mark those from that paper.

The single top t-channel cross section of 90 pb at $\sqrt{s} = 8$ TeV obtained at the LHC [89] is substantially larger than at the Tevatron and thus provides large samples of individual top quark events. An interesting feature of the LHC is that about twice as many top as antitop quarks are produced due to the proton–proton initial state (these numbers are the same for the Tevatron). All measured single top quark production cross sections and ratios of the top to antitop cross sections at 7 TeV and 8 TeV LHC energies are in agreement with SM predictions. The s-channel cross section calculated in the SM (3.2 pb at $\sqrt{s} = 7$ TeV [90]) is slightly bigger than that of the Tevatron, as this process requires quark–antiquark annihilation (see Fig. 7), which is provided by only sea antiquarks at the LHC. As backgrounds for the s-channel process increase rapidly with energy, this channel has not yet been observed at the LHC. In addition to s-channel and t-channel productions, single top quarks can be produced in association with a W-boson, called the tW-channel, as shown in Fig. 11. The cross section for this process is 22 pb at 8 TeV [91]. While this cross section is

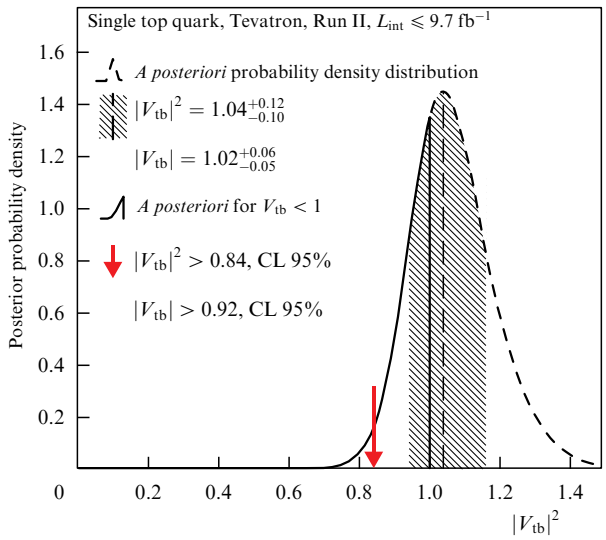

Figure 10. *A posteriori* probability distribution as a function of $|V_{tb}|^2$ for the combination of CDF and D0 results.

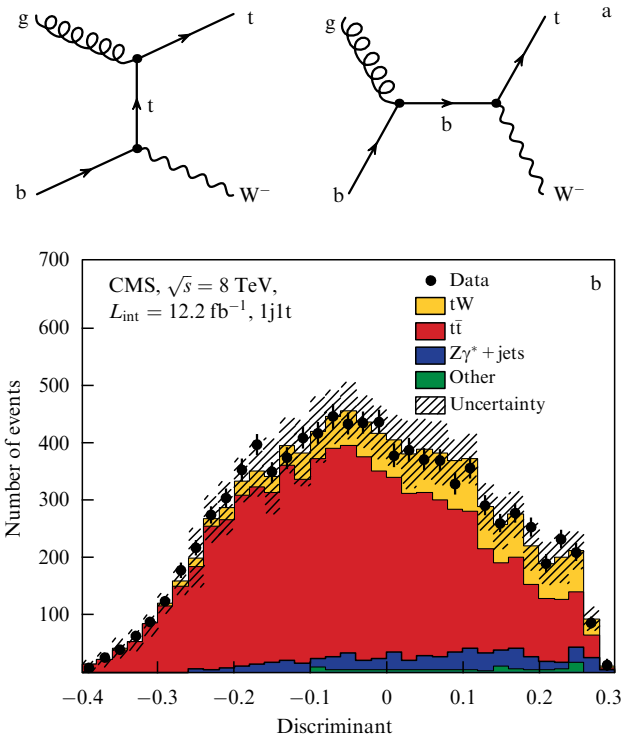

Figure 11. (Color online.) Leading order Feynman diagrams of associated W-boson and top quark production (a), and CMS observation of the associated tW production (b).

substantial, top-quark pair production creates a substantial background. The CMS experiment, using 12 fb^{-1} of $\sqrt{s} = 8$ TeV collisions and multivariate analysis methods, was able to observe tW associated production with 6.1σ significance, completing the observation of all leading order processes accompanying single top quark production [92].

6. Top-quark mass

6.1 Direct measurements

Measurements of the top-quark mass, $m_{\rm t}$, using kinematic properties of the decay products of the top quark, i.e., using *direct* approaches, have been performed by the ATLAS, CDF, CMS, and D0 Collaborations applying a variety of experimental techniques, which can be grouped into three categories:

• *The template method* relies on probability densities (PDs), often referred to as 'templates', of the distributions of kinematic observables related to the top-quark mass, such as the invariant mass of the trijet system from the $\rm t \to q\bar{q}'b$ decay. The templates are constructed using simulated MC events, where the signal templates are parametrized as a function of $m_{\rm t}$ and possibly other parameters, such as the jet energy correction factors. The sensitivity to $m_{\rm t}$ is established by comparing the distribution(s) of selected observable(s) in data to the templates as a function of $m_{\rm t}$ and possibly other parameters, for example, with a maximum likelihood fit.

• *The matrix element method* proceeds from *ab initio* calculations of the PD $P_{\rm evt}$ as a function of $m_{\rm t}$ and possibly other parameters for a given event to be observed under the hypotheses of top quark production, $P_{\rm sig}$, or of a background process, $P_{\rm bgd}$, where $P_{\rm evt} = f P_{\rm sig} + (1-f) P_{\rm bkg}$ and f is the fraction of signal events in the sample, determined from data. The $P_{\rm sig}$ and $P_{\rm bgd}$ PDs are expressed through their respective matrix elements (MEs) $M_{\rm sig}$ and $M_{\rm bgd}$, taking into account the experimental resolutions of the jets and leptons measured in the detector. The MEs are sums over all contributors at a given order. Typically, all possible jet–parton assignments are considered and weighted by their consistency with b-tagging information. The method establishes the sensitivity to $m_{\rm t}$ by calculating $P_{\rm evt}$ as a function of $m_{\rm t}$ and maximizing the combined likelihood for all observed events.

• *The ideogram method* can be considered an approximation to the ME method, since it also calculates a per-event PD under the $\rm t\bar{t}$ production and background hypotheses. In contrast to the ME method, $P_{\rm sig}$ is calculated based on a kinematic fit of the decay products of the top quark to its Breit–Wigner resonance within their respective experimental resolutions. All possible jet–parton assignments are summed, typically weighted by their consistency with the b-tagging information, and by the negative logarithm of the χ^2 of their kinematic fit. The combined likelihood of all observed events is then maximized to establish the sensitivity to $m_{\rm t}$.

The advantage of the template method resides in the fact that it is intuitive and straightforward in the sense that no calibration of the analysis is needed, since the templates are constructed directly from simulated MC events. This was the method used to estimate the top-quark mass in the discovery papers [1, 2].

The advantage of the ME technique is that it provides the highest possible statistical sensitivity according to the Neyman–Pearson lemma [93] by analyzing the full four-vectors of the measured final-state objects under *fundamental* signal and background hypotheses. It also provides a more accurate estimation of systematic uncertainties, as it evaluates their impact following a concrete model described by $|M_{\rm sig}|^2$, $|M_{\rm bkg}|^2$, and the experimental resolutions. A disadvantage of the ME method lies in its high computational demand. The ideogram method has the advantage that it is considerably less computationally demanding than the ME method.

A summary of the most precise recent direct measurements of $m_{\rm t}$ from the ATLAS, CDF, CMS, and D0 Collaborations is given in Table 2, and an overview of the measured values is presented in Fig. 12. In the following, we review three representative measurements using the three above-mentioned experimental techniques.

ATLAS recently performed a measurement of $m_{\rm t}$ in the *ll* channel in pp collisions at $\sqrt{s} = 7$ TeV using 4.7 fb^{-1} of integrated luminosity [94]. This analysis applied a template method to the $m_{\rm lb}$ observable, which is defined as the average invariant mass of the charged lepton $\rm l^{\pm}$ and the b-quark from the $\rm t \to W(\mathit{l}^{+}\nu)\,b$ and $\rm \bar{t} \to W(\mathit{l}^{-}\nu)\,\bar{b}$ decays. This observable was found to exhibit less dependence on systematic uncertainties than other observables [106]. The result was $m_{\rm t} = 173.79 \pm 0.54({\rm stat.}) \pm 1.30({\rm syst.})$ GeV.

A measurement of $m_{\rm t}$ in the l + jets channel in pp collisions at $\sqrt{s} = 8$ TeV was carried out by CMS using 19.7 fb^{-1} of integrated luminosity [102]. The analysis was performed applying the ideogram method. Like most measurements of $m_{\rm t}$ in the l + jets and all-jets channels, this analysis performs an *in situ* calibration of the overall jet energy scale correction factor, $k_{\rm JES}$, by constraining the invariant mass of the dijet system associated with the resulting $\rm W \to q'\bar{q}$ decay to $m_{\rm W} = 80.4$ GeV [107]. The top-quark mass was $m_{\rm t} = 172.04 \pm 0.19({\rm stat.}) \pm 0.75({\rm syst.})$ GeV.

Table 2. Overview of recent direct* measurements of m_t.

Experiment	Channel	Method**	Energy, TeV	$\int L\,dt$, fb^{-1}	$m_t \pm$ (stat.)$\pm$(syst.), GeV	Uncertainty, %	References
ATLAS	ll & l + j	Template	7	4.7	$172.99 \pm 0.48 \pm 0.78$	0.53	[94]
	single t	Template	8	20.3	$172.2 \pm 0.7 \pm 2.0$	1.2	[95]
	all jets	Template	7	4.7	$175.1 \pm 1.4 \pm 1.2$	1.1	[96]
CDF	ll	Template	1.96	9.1	$170.80 \pm 1.83 \pm 2.69$	1.90	[97]
	l + jets	Template	1.96	8.7	$172.85 \pm 0.71 \pm 0.85$	0.64	[98]
	all jets	Template	1.96	9.3	$175.07 \pm 1.19 \pm 1.56$	1.12	[99]
	E_T + j	Template	1.96	8.7	$173.93 \pm 1.64 \pm 0.87$	1.07	[100]
CMS	ll	Template	8	19.7	$172.3 \pm 0.3 \pm 1.3$	0.7	[101]
	l + jets	Ideogram	8	19.7	$172.04 \pm 0.19 \pm 0.75$	0.45	[102]
	all jets	Ideogram	8	18.2	$172.08 \pm 0.27 \pm 0.86$	0.52	[103]
D0	ll	Template	1.96	9.7	$173.32 \pm 1.36 \pm 0.85$	0.93	[104]
	l + jets	ME	1.96	9.7	$174.98 \pm 0.41 \pm 0.63$	0.43	[105]

* Only the most precise measurement in a given channel is shown for each experiment. The channel labelled as ll & l + j combines the results in the ll and l + jets channels. The label 'single t' stands for topologies enriched with the production of single top quarks. The channel labelled as E_T + j corresponds to l + jets events where the charged lepton is missed.
** ME — matrix element method.

The current most precise single measurement of m_t was carried out by D0 team in the l + jets channel in $p\bar{p}$ collisions at $\sqrt{s} = 1.96$ TeV using 9.7 fb^{-1} of integrated luminosity [105, 108]. This analysis applied an improved implementation of the ME method [109], which requires only 1% of the computation time needed previously [110]. This measurement substantially reduced the overall uncertainty relative to the previous measurement [110] through an improved estimation of the dominant uncertainties from the modeling of $t\bar{t}$ events and of the detector response. As shown in Fig. 13a, a simultaneous fit to m_t and the jet energy scale factor k_{JES} was made using the W-boson mass constraint. The result was $m_t = 174.98 \pm 0.41(\text{stat.}) \pm 0.63(\text{syst.})$ GeV.

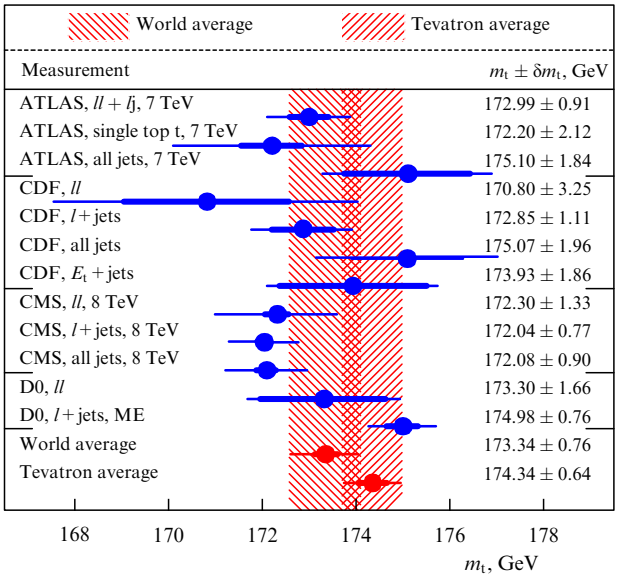

Figure 12. Overview of recent direct measurements of m_t. Only the most precise measurement in a given channel is shown for each experiment. The statistical uncertainty is indicated by the thick inner error bars, while the total uncertainty is marked by the thin outer error bars. The uncertainty given as δm_t represents the total uncertainty. For references to the measurements see Table 2.

The first world combination of m_t measurements was performed in 2014 using the best linear unbiased estimator (BLUE) code [111, 112] and taking into account the correlations among the colliders, experiments, and analysis channels for all sources of systematic errors considered [10]. The combined value was $m_t = 173.34 \pm 0.27(\text{stat.}) \pm 0.71(\text{syst.})$ GeV, which corresponds to a relative error of 0.44%. Many of the recent measurements listed in Table 2 were not included in Ref. [10], and substantial improvement is expected for the next world combination.

Currently, the world's most precise direct experimental determination of m_t comes from the recent Tevatron combination, which includes all results from the CDF and D0 Collaborations given in Table 2 except Ref. [104], and in addition includes the m_t results from Run I of the Tevatron at $\sqrt{s} = 1.8$ TeV [113]. The combination is performed with BLUE using a similar categorization of systematic errors to that of the world combination. The combined Tevatron result of $m_t = 174.34 \pm 0.37(\text{stat.}) \pm 0.52(\text{syst.})$ GeV corresponds to a relative error of 0.37%.

6.2 Indirect measurements

For a free particle with four-momentum p, the physical mass is usually taken as the pole of its propagator $1/[p^2 - (m^{\text{pole}})^2]$. Because of confinement, quarks cannot exist as free particles, and this definition becomes uncertain at the level of $\Lambda_{\text{QCD}} \approx 0.2$ GeV [114–116]. An alternative mass definition, $m_t^{\overline{\text{MS}}}$, is given in the modified minimal subtraction renormalization scheme [117]. The $m_t^{\overline{\text{MS}}}$ mass is also often referred to as the 'running mass' $m_t(\mu_R)$, which alludes to the main idea of absorbing the logarithmic corrections from soft QCD effects into the explicit dependence on the renormalization scale μ_R, resulting in a better numerical behavior of perturbative predictions. Other mass definitions have also been suggested [118, 119].

All direct measurements of m_t rely on simulated MC events, and therefore on the mass parameter used in MC event generators, m_t^{MC}. This introduces a dependence of the directly measured m_t on the theory model used to describe the showering of final state quarks or gluons and the subsequent hadronization process. As a result, m_t^{MC} is subject to a systematic uncertainty on the order of Λ_{QCD} [120], which is

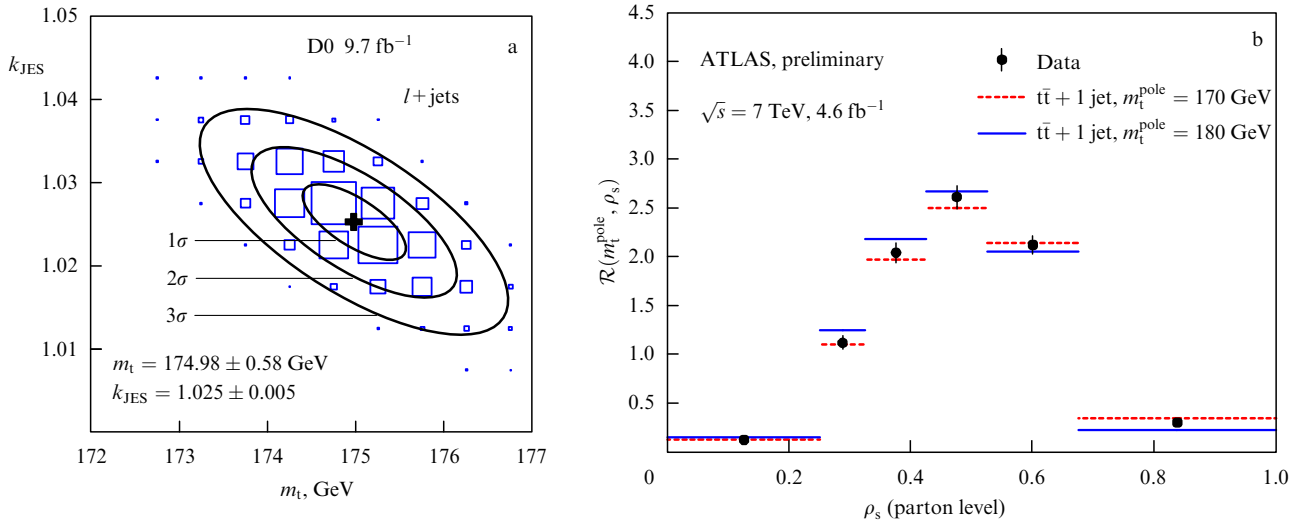

Figure 13. Two-dimensional likelihood in $m_{\rm t}$, $k_{\rm JES}$ for the world's most precise direct measurement of $m_{\rm t}$ [105] is shown in figure (a). Fitted contours of equal probability are overlaid as solid lines. The maximum is marked with a cross. The measured values with purely statistical uncertainties are given, where the statistical uncertainty from $k_{\rm JES}$ is propagated to the uncertainty in $m_{\rm t}$. The distribution $(1/\sigma_{t\bar{t}+1\rm jet})\,{\rm d}\sigma_{t\bar{t}+1\rm jet}/{\rm d}\rho_{\rm s}$, denoted as $\mathcal{R}$, is presented in figure (b) at the parton level for the world's most precise single measurement of $m_{\rm t}^{\rm pole}$ [127]. The dashed and continuous lines correspond to the SM expectation for $m_{\rm t}^{\rm pole} = 170$ and 180 GeV, respectively. The uncertainties shown in figures (a) and (b) are purely statistical.

explicitly accounted for in the measurements. The numerical values of $m_{\rm t}$ in the different definition schemes can differ significantly. For example, at NNLO, the difference between $m_{\rm t}^{\rm pole}$ and $m_{\rm t}^{\rm MS}$ is ~ 10 GeV. The $m_{\rm t}^{\rm MC}$ definition in state-of-the-art MC generators does not absorb any corrections from parton showering or hadronization, and therefore corresponds approximately to $m_{\rm t}^{\rm pole}$, with an ambiguity of up to 1 GeV [119, 120].

The first indirect measurements of $m_{\rm t}$ that avoided the ambiguity between $m_{\rm t}^{\rm MC}$ and $m_{\rm t}^{\rm pole}$ were performed by CDF [121] and D0 [122] in 2008. These measurements extracted $m_{\rm t}^{\rm pole} = 178^{+11}_{-10}$ GeV and $m_{\rm t}^{\rm pole} = 170 \pm 7$ GeV from the top-quark pair production cross section, $\sigma_{t\bar{t}}$, measured in the ll (CDF) and $j+$jets (D0) channels using integrated luminosities of 1.2 and 0.9 fb^{-1}, by relating the experimental results to the NLO [123] and approximate NNLO [38] predictions, respectively.

The world's most precise single measurement of $m_{\rm t}^{\rm pole}$ from $\sigma_{t\bar{t}}$ was performed with an uncertainty of 2.6 GeV by ATLAS in the eμ channel using pp collision data at $\sqrt{s} = 7$ and 8 TeV [124]. This measurement profits from a small experimental error of $\approx 4\%$ and the advent of the complete NNLO calculation of $\sigma_{t\bar{t}}(m_{\rm t}^{\rm pole})$ [38], including next-to-next-leading logarithmic (NNLL) corrections, which has a substantially reduced uncertainty relative to the approximate NNLO results. A similar measurement was performed by CMS, which achieved an uncertainty of 2.9 GeV [125].

Recently, ATLAS applied a novel approach [126] to measure $m_{\rm t}^{\rm pole}$ from the production cross section of $t\bar{t}$ events in association with a hard jet, $\sigma_{t\bar{t}+1\,\rm jet}$ [127], as a function of the inverse of the invariant mass of the $t\bar{t}+1$ jet system, $\rho_{\rm s} \propto 1/\sqrt{s_{t\bar{t}+1\,\rm jet}}$, and achieved an $m_{\rm t}^{\rm pole}$ measurement accuracy of 2.2 GeV. The normalized unfolded distribution $1/\sigma_{t\bar{t}+1\,\rm jet}({\rm d}\sigma_{t\bar{t}+1\,\rm jet}/{\rm d}\rho_{\rm s})$ is compared with NLO calculations

Table 3. Overview of recent indirect measurements of $m_{\rm t}^{\rm pole}$.

Experiment	Channel*	From cross section	Energy, TeV	$\int L\,{\rm d}t$, fb^{-1}	$m_{\rm t}$, GeV	Uncertainty**, %	References	
							Experiment	Theory
ATLAS	eμ	$\sigma_{t\bar{t}}$	7	4.6	$171.4^{+2.6}_{-2.6}$	$^{1.5}_{-1.5}$	[123]	[37]
	eμ	$\sigma_{t\bar{t}}$	8	20.3	$174.1^{+2.6}_{-2.6}$	$^{1.5}_{-1.5}$	[123]	[37]
	$l+$jets	$\sigma_{t\bar{t}+1\,\rm jet}$	7	4.6	$173.7^{+2.3}_{-2.1}$	$^{1.3}_{-1.2}$	[126]	[125]
CDF	ll	$\sigma_{t\bar{t}}$	1.96	1.2	$178.3^{+10.9}_{-9.9}$	$^{6.1}_{-5.5}$	[120]	[122]
CMS	ll	$\sigma_{t\bar{t}}$	7	2.3	$176.7^{+3.0}_{-2.8}$	$^{1.7}_{-1.6}$	[124]	[37]
D0	ll & $l+$j	$\sigma_{t\bar{t}}$	1.96	9.7	$169.4^{+3.6}_{-3.8}$	$^{2.1}_{-2.2}$	[40]	[37]

* The channel labelled as ll & $l+$j combines the results in the ll and $l+$jets channels.
** The total uncertainty quoted corresponds to the quadratic sum of the total experimental uncertainty and the entire uncertainty of theory.

[126] as a function of m_t^{pole} in Fig. 13b. Recent measurements of m_t^{pole} are summarized in Table 3.

7. Top-quark properties

Unlike the top-quark mass, the SM predicts all other properties of top quarks and their decays with high precision. Since the top-quark lifetime is much shorter than the time required for hadronization, top-quark properties can be measured directly and usually with much less uncertainty than those for other quarks. where these characteristics are derived from their bound states. Differences between measured properties and the precisely known SM predictions offer sensitive tests for new physics beyond the SM.

7.1 Top-quark lifetime

The lifetime τ and the related resonance width $\Gamma = \hbar/\tau$ are primary characteristics of any particle. Due to its large mass, a small value of the top lifetime, τ_t, is expected. The SM predicts $\Gamma_t = 1.32$ GeV [128] with about 1% uncertainty, or $\tau_t = 4.99 \times 10^{-25}$ s. It is impossible to measure such a short lifetime directly by measuring the distance between sites of birth and decay as done, for example, for B-mesons; nevertheless the CDF Collaboration undertook such a measurement, finding $\tau_t < 2 \times 10^{-13}$ s [129].

An alternative approach used for strongly interacting decays is a direct measurement of the mass spectrum width Γ. To use this method, the experimental mass resolution of the instrument should be better than the expected width. Unfortunately, all Tevatron and LHC experiments have mass resolutions worse than the SM Γ_t value. The most precise measurement of the top-quark width was taken by CDF [30] using 8.7 fb^{-1} of data. They obtain $1.10 < \Gamma_t < 4.05$ GeV, corresponding to $1.6 \times 10^{-25} < \tau_t < 6.0 \times 10^{-25}$ s at a 68% confidence level (CL), in agreement with the SM prediction.

The D0 Collaboration applied an indirect method to obtain Γ_t [131] under the assumption that $\Gamma(t \to Wb)$ is proportional to the measured t-channel single top quark production cross section with the proportionality factor equal to

$$\frac{\Gamma(t \to Wb)_{SM}}{\sigma(\text{t-channel})_{SM}},$$

as predicted by the SM. The width is then obtained from the ratio $\Gamma_t = \Gamma(t \to Wb)/Br(t \to Wb)$, where $Br(t \to Wb)$ is the branching ratio for $t \to Wb$. Using the experimental values of $\sigma(\text{t-channel}) = 2.90 \pm 0.59$ pb [132], and $Br(t \to Wb) = 0.90 \pm 0/04$ [133], as well as the SM predictions $\Gamma(t \to Wb) = 1.33$ GeV [107] and $\sigma(\text{t-channel}) = 2.14 \pm 0.18$ pb [81], they obtained $\Gamma_t = 2.00^{+0.47}_{-0.43}$ GeV and $\tau_t = 3.29^{+0.90}_{-0.63} \times 10^{-25}$ s. This indirect method was also implemented by CMS [134] with parameters from Refs [107, 134–136] to obtain $\Gamma_t = 1.36 \pm 0.02(\text{stat})^{+0.14}_{-0.11}(\text{syst})$ GeV, in good agreement with the SM prediction.

7.2 t and $\bar{t}$ mass difference

The CPT theorem based on the general principles of local relativistic quantum field theory predicts that antiparticle properties are the same as the corresponding particle properties after spatial and time coordinate inversions. In particular, particle and antiparticle masses must be the same. Although CPT symmetry is rigorously conserved in the SM, some SM extensions permit CPT invariance breaking [137–139]. A stringent limit on particle–antiparticle mass inequality was obtained for the $K^0 - \overline{K^0}$ system, namely

$$\frac{m_{K^0} - m_{\overline{K^0}}}{m_{K^0}} < 0.6 \times 10^{-18},$$

at a 90% CL [107], but some SM extensions allow different quark flavors to have vastly different CPT-violating couplings. The experimental results given in Table 4 are in good agreement with invariance under the CPT transformation. In these measurements, the identification of top or antitop quarks is achieved by measuring the change of the lepton from the W-boson in $t \to Wb$.

Table 4. Mass differences of top and antitop quarks measured at the Tevatron and the LHC.

Experiment	$m_t - m_{\bar{t}}$, GeV	References
D0	$0.8 \pm 1.8(\text{stat.}) \pm 0.5(\text{syst.})$	[140]
CDF	$-1.95 \pm 1.11(\text{stat.}) \pm 0.59(\text{syst.})$	[141]
CMS	$-0.44 \pm 0.46(\text{stat.}) \pm 0.27(\text{syst.})$	[142]
ATLAS	$0.67 \pm 0.61(\text{stat.}) \pm 0.41(\text{syst.})$	[143]

7.3 Top-quark electric charge

In the SM, the top quark possesses an electric charge $+(2/3)\,e$ and decays to W^+ and a charge $-(1/3)\,e$ quark (dominantly b-quark). But in an extension of the SM [144, 145], an exotic quark with a mass of about 170 GeV and charge of $-(4/3)\,e$ occurs as part of a fourth quark generation with decay to W^-b, while the SM top-quark mass is expected to be heavier than 230 GeV. The first constraint on a $-(4/3)\,e$ top quark was obtained by D0 in 2007 [146]; more recently, D0 reported [47] the analysis of 286 fully reconstructed $t\bar{t}$ pairs in the $l+$jets channel. The results demonstrated in Fig. 14a rule out an exotic $-(4/3)\,e$ top quark at a significance greater than 5σ and set an upper bound on the exotic quark fraction of 0.46 at 95% CL.

The CDF Collaboration performed an analysis in the $l+$jets channel [148]. The W-boson charge Q_W was determined from the decay lepton charge. The associated hadron jet charge Q_{jet} was reconstructed with a special jet charge algorithm. A negative value of the product $Q_W Q_{jet}$ corresponds to the SM $t\bar{t}$ decay, while its positive sign comes from the exotic $t\bar{t}$ decays. The results shown in Fig. 14b exclude an exotic top quark with a $-(4/3)\,e$ charge and mass of about 170 GeV at the 99% CL

The most stringent constraint on the existence of a $-(4/3)\,e$ quark with mass of about 170 GeV was given by ATLAS [149]. The results obtained are shown in Table 5. The data for the e- and μ-channels are in good agreement and coincide with the SM prediction of $(2/3)\,e$ within the errors quoted. They exclude the XM model [144] with a significance of more than 8σ. This model disagrees with the results on single top production as well [150, 151].

7.4 W-boson polarization in top-quark decays

The helicities of W-bosons in top-quark decays can be +1, −1, or 0, corresponding to right-handed, left-handed, or longitudinal polarizations, with corresponding fractions f_+, f_-, or f_0 of events in the decay $t \to Wb$, respectively. These fractions can be measured using the event distribution over $\cos\theta^*$ [152], where θ^* is the angle between the charged lepton

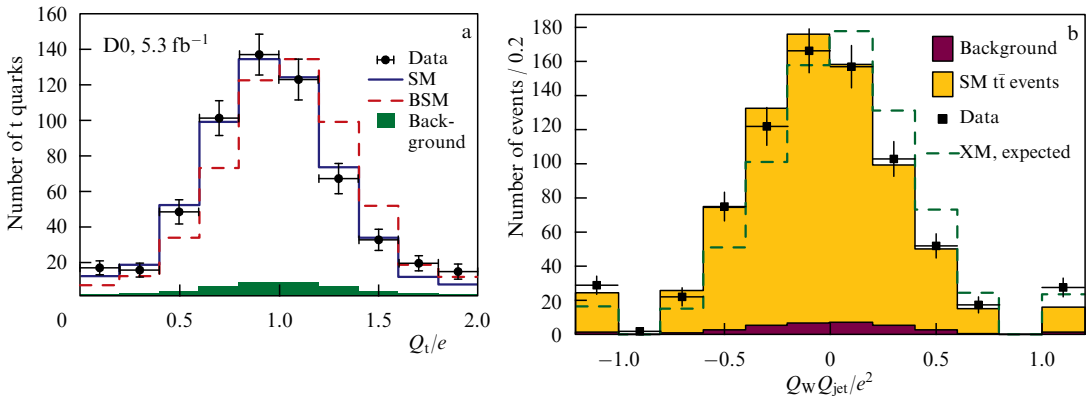

Figure 14. (Color online.) (a) Combined distributions in the charge Q_t for $t\bar{t}$ candidates in D0 data compared with expectations from the SM and the BSM taken from Ref. [147]. The background contribution is represented by the green-shaded histogram. (b) Distribution of the product of the W-boson charge times the jet charge from CDF. The shaded histograms give signal and background predictions. The dashed line shows the expectation from an exotic model (XM) [144, 145]. SM-like candidates are on the negative side of the abscissa axis, while XM-like candidates are on the positive side. The outermost bins correspond to the cases where $Q_{jet} = \pm 1$.

Table 5. ATLAS results of the top-quark charge (Q_t) measurements.

Channel	Q_t/e
e + jets	$0.63 \pm 0.04(\text{stat.}) \pm 0.11(\text{syst.})$
μ + jets	$0.65 \pm 0.03(\text{stat.}) \pm 0.12(\text{syst.})$
Combination of channels	$0.64 \pm 0.02(\text{stat.}) \pm 0.08(\text{syst.})$

momentum and the negative of the top-quark momentum in the W-boson rest frame (see Fig. 15):

$$\frac{1}{\sigma}\frac{d\sigma}{d\cos\theta^*} = \frac{3}{4}(1-\cos^2\theta^*)f_0 + \frac{3}{8}(1-\cos\theta^*)^2 f_- + \frac{3}{8}(1+\cos\theta^*)^2 f_+ .$$

The SM predicts $f_0 = 0.687 \pm 0.005$, $f_- = 0.3117 \pm 0.005$, and $f_+ = 0.0017 \pm 0.0001$ [153]. Deviations from these values would indicate new physics beyond the SM.

Appropriate findings are presented in Table 6 and Fig. 16. The experimental results are consistent and agree well with SM expectations for helicity fractions, and with the V−A structure of the Wtb vertex.

7.5 CKM matrix element V_{tb}

In the SM, the 3 × 3 unitary CKM matrix [11, 12] describes quark mixing. The measurement of $|V_{tb}|$ is based on the relation

$$R = \frac{\text{Br}(t \to Wb)}{\sum_q \text{Br}(t \to Wq)} = \frac{|V_{tb}|^2}{\sum_q |V_{tq}|^2} ,$$

where q is any down type quark. Due to the unitarity condition, $\sum_q |V_{tq}|^2 = 1$, and thus $R = |V_{tb}|^2$. A global fit to the SM parameters gives $|V_{tb}| = 0.999146^{+0.000021}_{-0.000046}$ [107]. Any experimental deviation from this value will be evidence of new BSM physics, for example, the existence of a fourth quark generation [158].

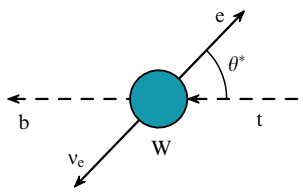

Figure 15. Definition of the helicity angle θ^*.

Table 6. Results of the helicity fraction (f) measurements.

Experiment	f	Results	References
D0 + CDF	f_0	$0.722 \pm 0.081(\pm 0.062(\text{stat.}) \pm 0.52(\text{syst.}))$	[154]
	f_+	$-0.033 \pm 0.046(\pm 0.034(\text{stat.}) \pm 0.31(\text{syst.}))$	
CDF	f_0	$0.726 \pm 0.066(\text{stat.}) \pm 0.067(\text{syst.})$	[155]
	f_+	$-0.045 \pm 0.044(\text{stat.}) \pm 0.058(\text{syst.})$	
ATLAS	f_0	0.67 ± 0.07	[156]
	f_-	0.32 ± 0.04	
	f_+	0.01 ± 0.05	
CMS	f_0	$0.720 \pm 0.039(\text{stat.}) \pm 0.037(\text{syst.})$	[157]
	f_-	$0.298 \pm 0.028(\text{stat.}) \pm 0.032(\text{syst.})$	
	f_+	$-0.018 \pm 0.019(\text{stat.}) \pm 0.011(\text{syst.})$	

The results of the R measurements are summarized in Table 7. The decay channels of the $t\bar{t}$ events selected for the analysis were l + jets and the dilepton in Ref. [133], l + jets in Ref. [159], and the dilepton in Refs [134, 160]. When restricting to $R \leqslant 1$, the $|V_{tb}|$ lower bound in Ref. [134] becomes equal to 0.955. All results are consistent with SM expectations.

The value of $|V_{tb}|$ can also be obtained from the single top production cross sections without the assumption of three quark generations or the unitarity of the CKM matrix, as discussed in Section 5.

8. Role of the top quark in the Standard Model

The top quark, as the weak isospin partner of the b-quark, plays an important role both in the SM and in its predictions for experiments. Here, we consider briefly several aspects of the role of top quarks: cancellations of chiral anomalies, flavor changing neutral currents and the GIM mechanism, the large top Yukawa coupling and consistency of the Higgs mechanism of spontaneous electroweak symmetry breaking

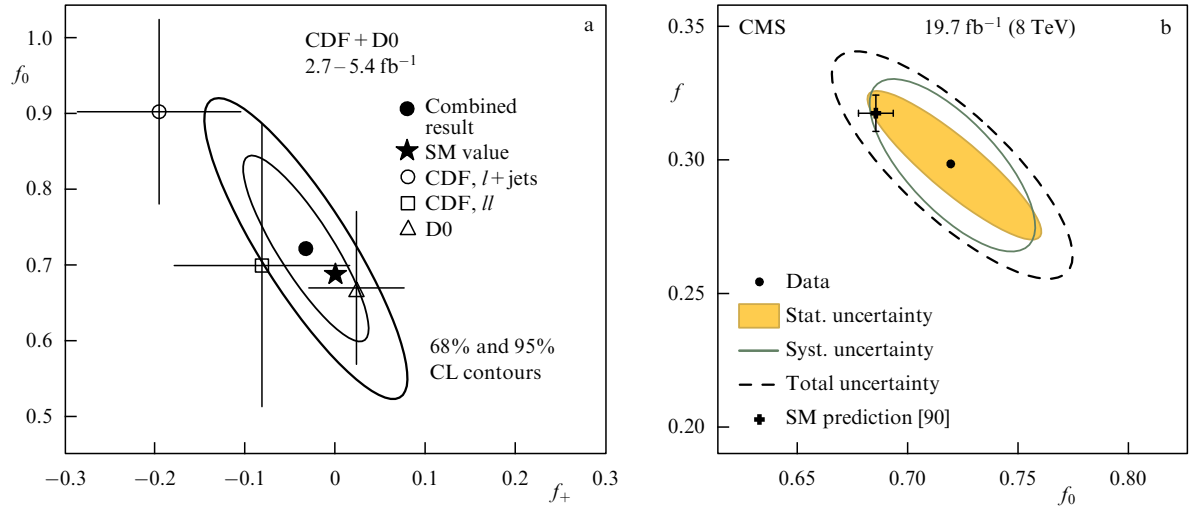

Figure 16. (a) Contours of constant χ^2 for the Tevatron combination of 2D helicity measurements [154]. The ellipses indicate the 68% and 95% CL contours, the dot shows the best-fit value, and the star marks the expectation from the SM. Each of the input measurements uses a central value of $m_t = 172.5$ GeV. (b) Combined results from the CMS muon + jets and electron + jets events for the left-handed and longitudinal W-boson helicity fractions [157], shown as 68% CL contours for statistical, systematic, and total uncertainties, compared to the SM predictions [153].

Table 7. Results of measurements of the ratio between R and $|V_{tb}|$ in $t\bar{t}$ events.

Experiment	R	$\lvert V_{tb}\rvert$	Lower limit at 95 % CL	References
D0	0.90 ± 0.04	0.95 ± 0.02		[133]
CDF	0.87 ± 0.07	0.93 ± 0.04	> 0.85	[159]
CDF	0.94 ± 0.09	0.97 ± 0.05	> 0.89	[160]
CMS	1.014 ± 0.032	—	> 0.975	[134]

[161–165], and large quantum corrections to electroweak observables.

8.1 Standard Model self-consistency: chiral anomalies

The top quark is needed for the consistency of the SM as a gauge quantum field theory. In the SM, the fermions, both leptons and quarks, are combined into three generations forming left-handed doublets and right-handed singlets with respect to the weak isospin $I_f^{L,R}$,

$$I_f^{L,R} = \pm\frac{1}{2}, 0 : \begin{array}{lll} \begin{pmatrix}\nu_e\\ e^-\end{pmatrix}_L, & e_R^-; & \begin{pmatrix}u\\ d\end{pmatrix}_L, \; u_R, d_R, \\ \begin{pmatrix}\nu_\mu\\ \mu^-\end{pmatrix}_L, & \mu_R^-; & \begin{pmatrix}c\\ s\end{pmatrix}_L, \; c_R, s_R, \\ \begin{pmatrix}\nu_\tau\\ \tau^-\end{pmatrix}_L, & \tau_R^-; & \begin{pmatrix}t\\ b\end{pmatrix}_L, \; t_R, b_R, \end{array}$$

where for any fermion field f the left and right chiral components are defined as

$$f_{L,R} = \frac{1}{2}(1 \mp \gamma_5) f.$$

In order to correctly reproduce the electromagnetic and weak interactions, the gauge group of the electroweak part of the SM is taken as

$$SU_L(2) \otimes U_Y(1), \qquad (2)$$

where $SU_L(2)$ is called the weak isospin group (the weak isospin is an analog of the usual isospin introduced by Heisenberg to describe the proton and the neutron), and $U_Y(1)$ is the weak hypercharge group. The hypercharges of the left- and right-handed lepton and quark fields are chosen such that the electric charges are equal to the known measured charges

$$Q_f = (T_3^f)_L + \frac{Y_L^f}{2}, \qquad Q_f = (T_3^f)_R + \frac{Y_R^f}{2}, \qquad (3)$$

where $(T_3^f)_{R,L}$ are the isospin projections equal to $+1/2$ for the up type component and $-1/2$ for the down type component of the fermions, and $Y_{L,R}^f$ stands for corresponding weak hypercharges of the fermions. These relations are known as the Gell-Mann–Nishijima formulas. The relations for the group generators guarantee that, after the spontaneous symmetry breaking, the gauge symmetry $SU_L(2) \otimes U_Y(1)$ reduces to the unbroken electromagnetic group $U_{em}(1)$.

Because of this chiral structure of the SM, there is a potential 'chiral' anomaly problem. Generically, anomalies in a field theory correspond to the situation where some symmetry is present at the level of a classical Lagrangian but is violated at the quantum loop level. Indeed, after a quantization of the SM, one finds that the left- and right-handed fermion currents, conserved in accord with the Nöther theorem at the classical level, are not conserved for individual leptons or quarks at the quantum level due to the triangle loop contributions shown in Fig. 17.

If an anomaly does not vanish, the theory loses its gauge invariance and, therefore, cannot be acceptable. (However, in

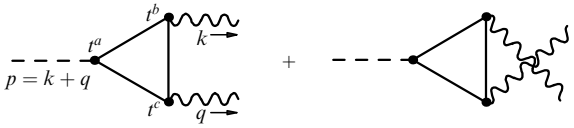

Figure 17. Loop corrections leading to anomalies. p, q, k are 4-momenta, and t^a, t^b, t^c are a generic notation for the gauge group generator at the interaction vertex of the corresponding gauge boson with the fermion in the loop.

the case of anomaly-free fundamental theories such as QED, one may consider some currents, for example, pseudoscalar fermion pair currents, that possess some global symmetry at the classical level in addition to the local gauge symmetries of the fundamental theory. Anomalies for such currents do not lead to problems. Moreover, this type of anomaly may have very important physics consequences, as in the case of the π^0-meson decay to two photons.) In the SM, the simultaneous contributions from left and right chiral fermions to anomalies occur with opposite signs. The anomaly is then proportional to the difference between traces of group generators coming from fermions with left and right chiralities:

$$\textit{Anomaly} \sim \mathrm{Tr}\left[t^a\{t^b t^c\}\right]_{\mathrm{L}} - \mathrm{Tr}\left[t^a\{t^b t^c\}\right]_{\mathrm{R}}, \tag{4}$$

where the square and the curly brackets denote commutators and anticommutators, respectively.

In theories like QED or QCD, there are no γ_5 matrices in the Lagrangians. Therefore, the left and right chiral contributions exactly compensate each other, so the anomaly is equal to zero and the theories make perfect sense.

In the electroweak part of the SM, left- and right-handed fermions couple to $\mathrm{U_Y}(1)$ gauge bosons with different hypercharges, and only the left components couple to the $\mathrm{SU_L}(2)$ gauge bosons. So, it is not obvious *a priori* that the chiral anomalies vanish. But the absence of anomalies is a requirement for the SM to be a valid quantum theory.

Without going into details (they can be found in textbooks; see, e.g., Refs [166–168]), one can check that all the chiral anomalies are cancelled in the SM for each fermion generation due to the simultaneous contributions of quarks and leptons with left and right chiralities. In particular, the cancellation of the anomaly in each generation takes place due to the sum of electric charges of leptons being equal in magnitude but opposite in sign to the sum of quark charges. For such a cancellation, the number of colors (N_{c}) must be equal to three. In particular, the cancellation for the third fermion generation requires a top quark with the charge $Q_{\mathrm{t}} = +2/3e$, giving $(Q_{\mathrm{t}} + Q_{\mathrm{b}})\, N_{\mathrm{c}} + Q_{\tau} = 0$.

8.2 Flavor changing neutral currents and the GIM mechanism

The basic principle in constructing the SM Lagrangian is gauge invariance which allows us to consider only two types of gauge-invariant terms describing quark–Higgs Yukawa interactions with mixing of the down and up quark fields from different generations:

$$L_{\mathrm{Yukawa}} = -\Gamma_d^{ij}\bar{Q}_{\mathrm{L}}^{\prime i}\Phi d_{\mathrm{R}}^{\prime j} - \Gamma_u^{ij}\bar{Q}_{\mathrm{L}}^{\prime i}\Phi^{\mathrm{C}} u_{\mathrm{R}}^{\prime j} + \mathrm{h.c.}, \tag{5}$$

where Γ_u^{ij}, Γ_d^{ij} are generic mixing coefficients for the upper and lower quark fields, respectively, $Q_{\mathrm{L}}^{\prime}$ is the left quark doublet in the form

$$Q_{\mathrm{L}}^{\prime} = \begin{pmatrix} u^{\prime} \\ d^{\prime} \end{pmatrix}_{\mathrm{L}},$$

with the symbol ($'$) used to account for quark states before rotation to the mass eigenstates, and the Higgs Φ and conjugate Higgs Φ^{C} fields in the unitary gauge have the forms

$$\Phi = \frac{1}{\sqrt{2}}\begin{pmatrix} 0 \\ v+h \end{pmatrix}, \quad \Phi^{\mathrm{C}} = \frac{1}{\sqrt{2}}\begin{pmatrix} v+h \\ 0 \end{pmatrix},$$

where $v = 246$ GeV is the vacuum expectation value of the Higgs field, and h is the scalar Higgs boson. After spontaneous symmetry breaking, the Lagrangian (5) takes the form

$$L_{\mathrm{Yukawa}} = -h\left[M_d^{ij}\,\bar{d}_{\mathrm{L}}^{\prime i}\,d_{\mathrm{R}}^{\prime j} + M_u^{ij}\,\bar{u}_{\mathrm{L}}^{\prime i}\,u_{\mathrm{R}}^{\prime j} + \mathrm{h.c.}\right]\left(1 + \frac{h}{v}\right),$$

where $M_{d,u}^{ij} = \Gamma_{d,u}^{ij} v/\sqrt{2}$ are mass mixing matrices for down and up quarks. The matrices should be diagonalized to get the physical states for up and down quarks. This can be done using unitary transformations in flavor space for all types of up and down and left and right quark fields:

$$d_{\mathrm{L}i}^{\prime} = (U_{\mathrm{L}}^{\mathrm{d}})_{ij}\, d_{\mathrm{L}j}, \quad d_{\mathrm{R}i}^{\prime} = (U_{\mathrm{R}}^{\mathrm{d}})_{ij}\, d_{\mathrm{R}j},$$

$$u_{\mathrm{L}i}^{\prime} = (U_{\mathrm{L}}^{\mathrm{u}})_{ij}\, u_{\mathrm{L}j}, \quad u_{\mathrm{R}i}^{\prime} = (U_{\mathrm{R}}^{\mathrm{u}})_{ij}\, u_{\mathrm{R}j}.$$

After such transformations, the above Yukawa Lagrangian will contain Dirac mass terms for quarks, and their interactions with the Higgs boson are proportional to the fermion masses:

$$L_{\mathrm{Yukawa}} = -\sum_{i=1}^{3}\left[m_d^i\,\bar{d}^i d^i + m_u^i\,\bar{u}^i u^i\right]\left(1 + \frac{h}{v}\right), \tag{6}$$

where $i = 1, 2, 3$ stands for three flavor generations and, in particular, m_u^3 is the top-quark mass m_{t}.

Recall that in the SM all fermion interactions with vector gauge fields follow from the gauge invariance principle and are expressed in terms of the products of the gauge fields with neutral and charged currents containing fermions from the same generation. Therefore, the above unitary transformations ($U^{\dagger}U = 1$) do not affect the neutral currents. As a result, there are no flavor changing neutral currents (FCNCs) in the SM at lowest order.

However, the charged currents

$$J_{\mathrm{C}}^{\mu} \sim \overline{u_{\mathrm{L}}^{\prime}}\gamma^{\mu} d_{\mathrm{L}}^{\prime} + \mathrm{h.c.}$$

contain quarks rotated by different unitary matrices for the up and down quarks:

$$u^{\prime} \to (U_{\mathrm{L}}^{u})\, u, \quad d^{\prime} \to (U_{\mathrm{L}}^{d})\, d.$$

After the unitary transformation, therefore, the charged current becomes

$$J_{\mathrm{C}}^{\mu} \sim (U_{\mathrm{L}}^{u})^{\dagger}\, U_{\mathrm{L}}^{d}\, \bar{u}_{\mathrm{L}}\gamma^{\mu} d_{\mathrm{L}}.$$

The unitary matrix is called the Cabbibo–Kobayashi–Maskawa mixing matrix [11, 12]:

$$V_{\mathrm{CKM}} = (U_{\mathrm{L}}^{u})^{\dagger}\, U_{\mathrm{L}}^{d},$$

$$V_{\mathrm{CKM}} = \begin{pmatrix} V_{\mathrm{ud}} & V_{\mathrm{us}} & V_{\mathrm{ub}} \\ V_{\mathrm{cd}} & V_{\mathrm{cs}} & V_{\mathrm{cb}} \\ V_{\mathrm{td}} & V_{\mathrm{ts}} & V_{\mathrm{tb}} \end{pmatrix}. \tag{7}$$

The CKM matrix is unitary since it is constructed from the product of unitary matrices. However, this is true only because of the presence of the top quark in the third generation.

The unitarity leads to various constraints on the elements of the CKM matrix, such as

$$\sum_{k=1}^{3} V_{ik}^{\dagger} V_{kj} = \delta_{ij}.$$

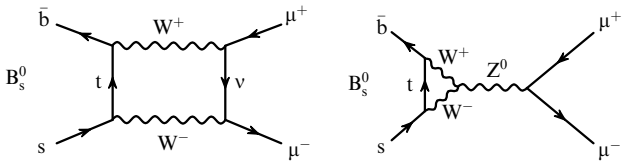

Figure 18. Box and Penguin loop diagrams contributing to the rare decay $B_s \to \mu^+\mu^-$.

One of the consequences of such unitary constraints is the GIM mechanism formulated originally for the case of two generations [7] but with obvious extension to three generations. The GIM mechanism allows one to understand flavor changing neutral current suppression at higher orders of perturbation theory in the SM. As explained above, the FCNCs are absent in the SM at the lowest order by construction. However, the FCNCs appear at higher orders in the case of two (real or virtual) W^+ and W^- emissions by the quark current. For example, the FCNC $b \to s$ transition is proportional to

$$V_{su}^{\dagger} V_{ub} S(p, m_u) + V_{sc}^{\dagger} V_{cb} S(p, m_c) + V_{st}^{\dagger} V_{tb} S(p, m_t)\,,$$

where $S(p, m_{u,\,c,\,t})$ is the propagator of the corresponding up quark with momentum p. In the case of equal quark masses, one would have the factor

$$V_{su}^{\dagger} V_{ub} + V_{sc}^{\dagger} V_{cb} + V_{st}^{\dagger} V_{tb}$$

in front of the current, which is equal to zero due to the unitary constraint. This is the exact GIM cancellation. If quark masses are not equal, as happens in nature, the FCNCs will be nonzero and will give well-defined predictions for various phenomena in the physics of K-, D- and B-mesons, such as oscillations, rare decays, etc. An example is the rare decay of the B_s-meson to a muon pair $\mu^+\mu^-$. Due to the absence of the FCNCs at the tree level, the leading Feynman diagrams are loop diagrams, called box and penguin, as shown in Fig. 18. In this case, the diagrams involving the virtual top quark dominate and lead to a theoretical decay rate of $B_s \to \mu^+\mu^-$ equal to $(3.66 \pm 0.23) \times 10^{-9}$ [169] in the SM, in good agreement with measured values by the LHCb [170] and the CMS [171] experiments.

We stress once again that the GIM mechanism works for three fermion generations only because of the existence of the top quark.

8.3 Top-quark Yukawa coupling and consistency of the Standard Model at high energy scales

As follows from Lagrangian (6), the Yukawa top–Higgs interaction is proportional to the top-quark mass:

$$L_{t\text{-}h} = -\frac{m_t}{v}\,\bar{t}th \tag{8}$$

and, therefore, it is strong, since the top-quark mass is large. The top Yukawa coupling

$$y_t = \frac{\sqrt{2} m_t}{v} \tag{9}$$

is numerically close to unity. Such a large top Yukawa coupling makes a significant impact on the Higgs potential, when higher order corrections are considered.

In the SM, as for any quantum field theory, all the masses and coupling constants get quantum corrections and become so-called running masses and running coupling constants. In particular, the Higgs boson self-interaction quartic coupling λ gets loop corrections coming from the top, Higgs, and electroweak gauge boson loops. As a result of the renormalization group evolution, λ becomes a function of the energy scale (renormalization scale μ). SM analyses of the running coupling constants are performed currently to NNLO accuracy [172–174].

Because of the running of the Higgs self-coupling constant, the behavior of the Higgs potential may be changed drastically at high-energy scales. Since the effective Higgs potential is proportional to $\lambda(\mu)$ at large μ or equivalently at a large value of the Higgs field, different situations may occur. The quartic coupling $\lambda(\mu)$ may be positive all the way up to the Planck scale, leading to an absolutely stable theory. On the other hand, $\lambda(\mu)$ may become negative at large μ, leading to a potential that falls with μ, leading to instability of the theory. Or $\lambda(\mu)$ may take such values that a second minimum of the potential appears at some particular scale, leading to metastability of the theory due to possible tunneling effects.

The second minimum takes place on some energy scale μ_0, where the derivative of $\lambda(\mu)$, or equivalently the β function, is zero:

$$\beta(\mu) = \left.\frac{d\lambda(\mu)}{d\ln\mu}\right|_{\mu=\mu_0} = 0\,. \tag{10}$$

If the value of the potential at the new minimum μ_0 is less than the value of the vacuum potential on the electroweak scale, then the theory is metastable. The boundary between stable and metastable cases corresponds to a situation where the first and second minima of the potential are equal. The minimum can always be chosen to be zero by a constant shift of the potential. This is equivalent to the condition

$$\lambda(\mu_0) = 0 \tag{11}$$

on some energy scale called the critical point $\mu_0 = M_{crit}$.

Because the largest loop corrections in the evolution of $\lambda(\mu)$ are proportional to various powers of the top Yukawa coupling y_t, the accurate measurement of the top-quark mass is of special importance. Results of the NNLO analysis are shown in Fig. 19 [174]. As can be seen, given the uncertainties, the second minimum and critical point could be achieved at the Planck scale. However, a top-quark mass of about 171.3 GeV is needed for this to occur. If the top-quark mass is heavier, the quartic coupling λ crosses zero at lower μ. In particular, the value of the top-quark mass close to the current measured value of $m_t = 173.1 \pm 0.6$ GeV leads to the scale $\mu \sim 10^{10}$ GeV for which the quartic coupling becomes negative.

Keeping in mind the relation between the Higgs mass and the quartic coupling $M_H^2 = 2\lambda v^2$, a bound is obtained for the Higgs mass, assuming the critical point to be the Planck scale [174]:

$$M_H\,[\text{GeV}] > 129.4 + 1.4\left(\frac{m_t[\text{GeV}] - 173.1}{0.7}\right) - 0.5\left(\frac{\alpha_s(m_Z) - 0.1184}{0.0007}\right) \pm 1.0_{th}\,, \tag{12}$$

where $\alpha_s(m_Z)$ is the running QCD coupling constant taken at the Z-boson mass m_Z, and 1.0_{th} GeV is an estimate of

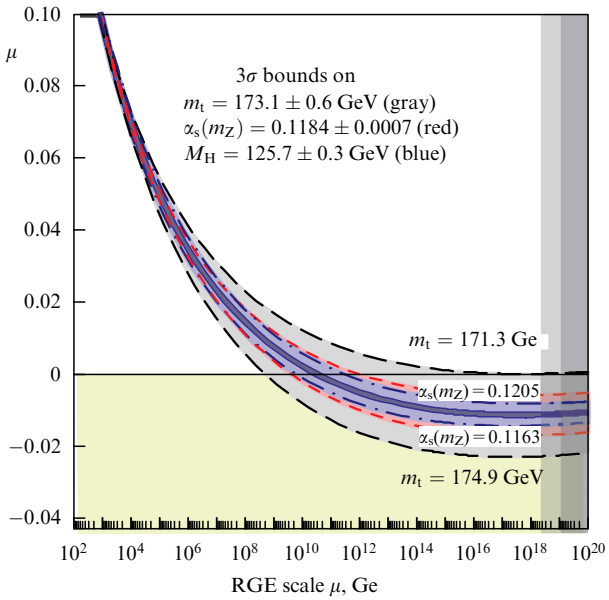

Figure 19. (Color online.) Renormalization group evolution of the quartic coupling λ. The bands correspond to variations of m_t, M_H and α_s at $\pm 3\sigma$ [174].

theoretical uncertainty of all loop computations involved. If we combine in quadrature the theoretical uncertainty and the experimental uncertainties on m_t and α_s, we get $M_H > 129.4 \pm 1.8$ GeV. Therefore, the conclusion from this analysis implies that the stability of the SM vacuum at energies up to the Planck scale is excluded for $M_H < 126$ GeV at 98% CL.

If the system of critical equations (10) and (11) is solved, boundaries for areas of stability, metastability, and instability may be found [174–176]. The result from Ref. [174] is shown in Fig. 20. The area defined by the current measured values and uncertainties in $\alpha_s(m_Z)$, m_t, and M_H is located in the metastability region, but close to the boundary with the stability region. However, the lifetime of such a metastable vacuum is estimated to be much larger than the current age of the Universe.

The exclusion of the SM as a valid quantum theory up to the Planck scale is only at the 2 sigma level with today's measured top quark and Higgs boson masses, so the hypothesis that the SM works all the way up to the Planck scale cannot be completely rejected. This allows scenarios with the SM Higgs acting as an inflaton to be considered [177, 178]. Clearly, a better precision of the top-quark mass is needed, as may be achieved at the LHC, but certainly at a future e^+e^- collider. As the precision of the top-quark mass measurement becomes substantially smaller than 1 GeV, it will become imperative that the measured mass have a well-defined theoretical meaning (see Section 6). Also, for demarcation between the stability, metastability, or criticality areas of the electroweak vacuum, a contribution from possible 'new physics' might be very important [179].

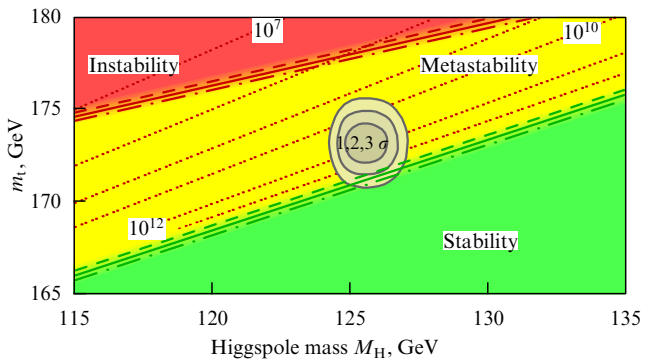

Figure 20. Regions of stability, metastability, and instability of the SM vacuum in the $m_t - M_H$ plane close to the experimentally allowed range of M_H and m_t at 1σ, 2σ, and 3σ. Boundary lines correspond to $\alpha_s(m_Z) = 0.1184 \pm 0.0007$ [174].

A large top mass and correspondingly large top Yukawa coupling lead to a potential problem with the SM called 'naturalness' or the 'hierarchy' problem. The loop corrections to the Higgs boson mass shown in Fig. 21 are given by the following leading expression:

$$\delta M_H^2 = \frac{3G_F}{4\sqrt{2}\pi^2}\left(2m_W^2 + m_Z^2 + M_H^2 - 4m_t^2\right)\Lambda^2 \approx -(0.2\Lambda)^2\,, \tag{13}$$

where the cutoff parameter Λ represents the possible 'new physics' scale. The main contribution to the correction comes from the top-quark loop.

The problem resides in the fact that correction (13) depends very strongly (quadratically) on the scale Λ, which may be related to contributions from the 'new physics'. If Λ is very large, (e.g., of the Planck scale order or somewhat less, say, around 10^{10} GeV), the Higgs mass on the order of 100 GeV is very unnatural. Such a dependence is a specific property of the scalar Higgs boson. Quadratic scale dependences for other SM particles are protected by symmetry — gauge symmetry for gauge bosons, and chiral symmetry for fermions, but there is no such SM symmetry protecting Higgs quadratic dependence.

If it is required that the correction to the Higgs mass be less than the Higgs mass itself, $\delta M_H < M_H$, the upper bound on the scale Λ will be found to be slightly less than 1 TeV (the 'little hierarchy' problem). No new physics particles on this mass scale have been found yet. But since the main contribution to the Higgs mass correction comes from the top loop, one might expect the existence of some rather light top-quark partners, such as stop quarks in supersymmetric models, making additional loop contributions which may cancel the top loop quadratic dependence on Λ [180–183].

8.4 Quantum corrections to electroweak observables

Because of the large top quark mass, one naively would think that the loop contributions from such a heavy particle would be suppressed. Indeed, in theories like QED or QCD the top-quark loop contributions are much smaller than those from light quarks. However, this is not true for the electroweak part of the SM. In previous sections, we have seen that, due to the large top Yukawa coupling, top loops are very important. For example, the main Higgs boson production channel at the

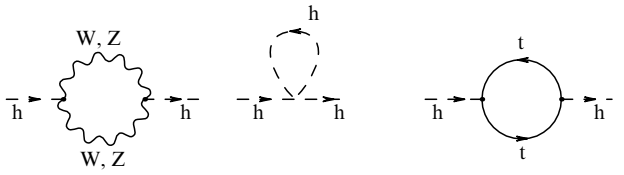

Figure 21. Loops contributing to the Higgs mass correction.

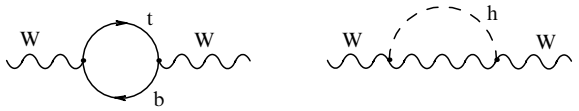

Figure 22. Loop corrections to the W-boson mass involving contributions from the top quark and the Higgs boson.

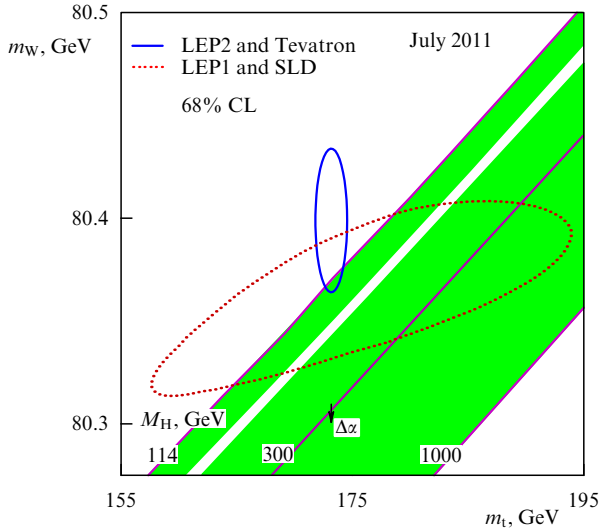

Figure 23. (Color online.) W-boson mass as a function of the top-quark mass at various values of the Higgs mass and the constraints on potential Higgs masses prior to the Higgs discovery. The open belt around $M_H = 160$ GeV had been excluded by the Tevatron experiments.

Tevatron or LHC, gluon–gluon fusion, proceeds mainly through a top-quark triangle diagram.

In the SM, the masses of the electroweak gauge bosons $W^{\pm}$ and Z appear due to the Higgs mechanism of spontaneous symmetry breaking, and the longitudinal components of the massive vector boson fields come from would-be Goldstone bosons. In the unitary gauge, the Goldstone bosons are 'eaten' by the longitudinal modes. Loop corrections to the electroweak observables are computed in covariant gauges where the interaction vertices of the Goldstone bosons with quarks are involved. These vertices contain terms proportional to the fermion masses and, therefore, the loops containing the top quark make the largest contributions. As an example, the loop correction to the W-boson mass shown in Fig. 22 due to top quarks depends quadratically on the top mass, while the Higgs boson loop correction depends logarithmically on the Higgs mass. Analysis of these mass corrections provided important constraints on the Higgs mass [184] prior to the Higgs discovery by confronting the measured m_t and m_W with calculations including these loop corrections, as shown in Fig. 23. These bounds pointed to the region where the Higgs was subsequently discovered at the LHC [185, 186].

The plot in the $m_W - m_t$ plane from the global fit of precision electroweak measurements by the SM loop level predictions [17] is shown in Fig. 24. The narrower blue and larger grey areas allowed at 1σ and 2σ correspond to cases when measurements of the Higgs boson mass are included in or excluded from the fit. These fits do not include the experimental m_W and m_t constraints. The allowed regions coincide well with the vertical and horizontal bands indicating the $\pm\sigma$ regions for the m_t and m_W direct measurements.

There are many other cases where the top loop contributions are large; for example, the partial decay width of the Z-boson to the $b\bar{b}$-quark pair or the rare B_s-boson decay to the $\mu^+\mu^-$ pair (see Section 8.2).

9. Top quark as a window to new physics

The top quark is the heaviest particle of the SM, which suggests that it may play a special role in the EW symmetry breaking (cf. Section 8). It also plays a central role in many Beyond the Standard Model (BSM) scenarios. This allows using the signatures in the production of pairs or single top quarks to search for such BSM scenarios. In Sections 9.1–9.5,

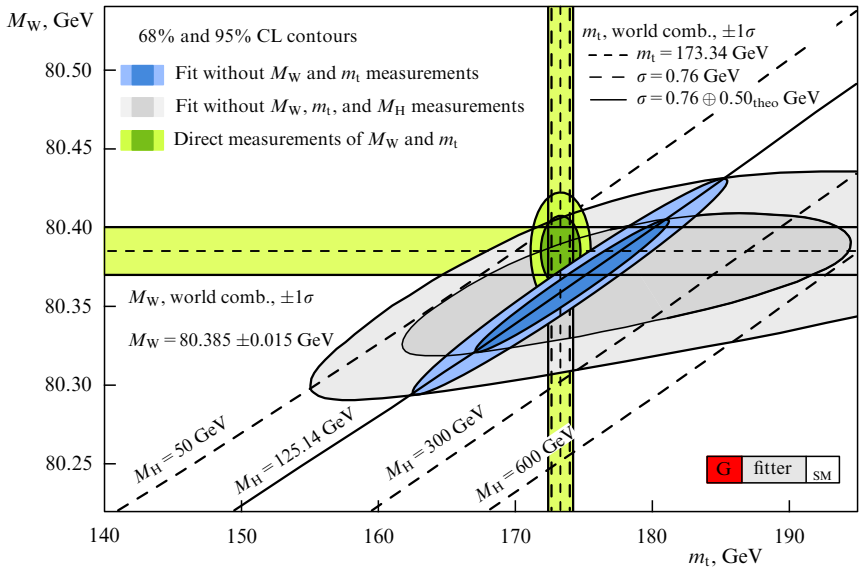

Figure 24. (Color online.) Two-dimensional plot for W-boson and top quark masses from the global fit of precision electroweak data excluding (grey area) and including (blue area) the Higgs mass measurements, to be compared with the directly measured values for the masses indicated by the horizontal and vertical belts.

we review the latest experimental results in which the top quark is used as a window to BSM physics.

9.1 Searches for associated $t\bar{t}$ production

In the SM, the top quark Yukawa coupling y_t is numerically within 1% of unity, given the world average value of $m_t = 173.34 \pm 0.76$ GeV [10]. A significant deviation of y_t from $y_t^{SM} \approx 1$ would be a clear indication of BSM-related phenomena. With the recent addition of the Higgs boson to the family of known particles, it became imperative to measure y_t directly, which can be accomplished using the associated production of a Higgs boson and a $t\bar{t}$ pair, where the Higgs boson is identified through the $H \to b\bar{b}$, $H \to \gamma\gamma$, $H \to WW$, or $H \to ZZ$ decay modes.

The first search for $t\bar{t}H(b\bar{b})$ production at a hadron collider was carried out in 2009 by D0 using $\mathcal{L} = 2.1$ fb^{-1} of data [187]. The best observed (expected) constraint at the Tevatron for $t\bar{t}H(b\bar{b})$ was $\mu < 17.6$ (12.4) in units of the SM expected cross section at a 95% CL, assuming $M_H = 125$ GeV; it was obtained by CDF using $\mathcal{L} = 9.4$ fb^{-1} of data [188]. The best constraints at the LHC came from the ATLAS and CMS Collaborations, both in the $t\bar{t}H(b\bar{b})$ mode. The ATLAS analysis applies a neural network discriminant and an ME method to $\mathcal{L} = 20.3$ fb^{-1} of data in the l + jets and dilepton channels, and obtains an observed (expected) upper bound of $\mu < 3.4(2.2)$ at a 95% CL [189]. Similarly, the CMS analysis obtains an observed (expected) bound of $\mu < 4.2(3.3)$ at a 95% CL by applying an ME method to $\mathcal{L} = 19.5$ fb^{-1} of data in the l + jets and dilepton channels [190]. The results correspond to a fitted $\mu = 1.5 \pm 1.1$ for ATLAS, and 1.2 ± 1.6 for CMS, consistent with the SM y_t value.

9.2 Searches for non-Standard Model Higgs bosons

Many BSM models, such as supersymmetry (see Section 9.3), predict an extended Higgs boson sector. The simplest extension, the 2 Higgs doublet model (2HDM) [191], postulates two complex $SU(2)_L$ doublet scalar fields rather than one in the SM. This results in eight degrees of freedom, three of which give masses to the SM W- and Z-bosons, while the remaining five manifest themselves as physical particles: two neutral scalars h and H, one pseudoscalar A, and two charged scalars $H^{\pm}$. Typically, h is assumed to correspond to the discovered Higgs boson. An important parameter of 2HDM models is the ratio of $\tan\beta$ of the vacuum expectation values of the two $SU(2)_L$ doublets. Large $\tan\beta$ results in enhanced couplings to third generation fermions of the SM. The couplings of $H^{\pm}$ bosons to SM particles are dominated by the $H^+t\bar{b}$ (and charge conjugate) vertex due to the large top-quark mass. Hence, searches for $H^{\pm}$ bosons concentrate on the $H^+ \to t\bar{b}$ process if $M_{H^{\pm}} > m_t$, and on $t \to H^+b$ if $M_{H^{\pm}} < m_t$.

The first search for $H^+ \to t\bar{b}$ was carried out by D0 using the s-channel single top-like process $p\bar{p} \to H^+ \to t\bar{b} \to W^+b\bar{b}$ using $\mathcal{L} = 0.9$ fb^{-1} of data [192]. Due to limited sensitivity, models with $\tan\beta < 100$ could not be excluded. CMS searched for $H^+ \to t\bar{b}$ through processes $pp \to H^+\bar{t}b \to \tau^+\nu\mu^+\nu\bar{b}b$ and $pp \to H^+\bar{t}b \to l^+\nu b\bar{b}l'^-\nu\bar{b}b$ using $\mathcal{L} = 19.5$ fb^{-1} of data [193], and upper bounds in the range of 180 GeV$< m + H^{\pm} <$ 600 GeV for $\tan\beta = 30$ have been placed.

Large values of $\tan\beta$ make the $H^+ \to \tau^+\nu$ decay mode favorable for $t \to bH^+$ searches, where the τ^+ lepton is typically identified through its hadronic decays. CDF searched for $H^+ \to \tau^+\nu$ decays in $t\bar{t}$-like topologies in the $t\bar{t}l$ + jets and ll channels through an enhancement of events with τ leptons using $\mathcal{L} = 0.2$ fb^{-1} of data [194]. Similar searches were conducted by D0 in the ll channel using $\mathcal{L} = 0.9$ fb^{-1} of data [195] and in the l + jets and ll channels using $\mathcal{L} = 1$ fb^{-1} of data [196]. Following the same strategy, ATLAS and CMS made searches for $t \to H^+b$ using $\mathcal{L} = 19.5$ fb^{-1} [197] and $\mathcal{L} = 19.7$ fb^{-1} [198] of data at $\sqrt{s} = 8$ TeV in l + jets and channels, respectively. In the absence of a BSM-related signal, upper bounds on $Br(t \to H^+b) \times Br(H^+ \to \tau^+\nu)$ were placed in the ($M_{H^{\pm}}$, $\tan\beta$)-plane down to $M_{H^{\pm}} = 80$ GeV.

The $H^+ \to c\bar{s}$ decay mode is favorable for small values of $\tan\beta$. The first search for this decay mode was conducted by CDF in $t\bar{t}$-like events in the l + jets channel, where the invariant mass of the non-b-tagged dijet system was used to discriminate $t \to H^+b$ against SM $t \to W^+b$ decays [199]. The same strategy was pursued by ATLAS using $\mathcal{L} = 4.7$ fb^{-1} of data at $\sqrt{s} = 7$ TeV [200], and by CMS with $\mathcal{L} = 19.7$ fb^{-1} at $\sqrt{s} = 8$ TeV [201]. D0 performed a simultaneous search for the $H^+ \to c\bar{s}$ and $H^+ \to \tau^+\nu$ decay modes by analyzing the l + jets and ll channels divided into regions according to the multiplicity of identified b-quark jets, using both hadronic and leptonic τ decays [202]. In the absence of a BSM signal, upper bounds on $Br(t \to H^+b) \times Br(H^+ \to c\bar{s})$ were placed in the ($M_{H^{\pm}}$, $\tan\beta$)-plane for $80 < M_{H^{\pm}} < 160$ GeV.

9.3 Searches for supersymmetric partners of the top quark

Supersymmetry [203] is widely considered to be a promising model for the extension of the SM. Its simplest version postulates a supersymmetric bosonic partner $\tilde{f}$ for each SM fermion f. A wide class of supersymmetric models predicts a natural dark matter candidate, which is typically the lightest neutralino mass eigenstate $\tilde{\chi}_1^0$ [203]. In the SM, the Higgs mass M_H receives loop contributions from each of the SM fermions, which can be orders of magnitude larger than M_H itself (cf. Section 8). This fine-tuning problem, also known as the hierarchy problem, can be elegantly resolved in supersymmetry, where the loop contribution of each f is cancelled by its superpartner $\tilde{f}$. The top-quark contribution to M_H is the largest due to $m_t \gg m_{f \neq t}$; hence, models with stop mass eigenstates $\tilde{t}_1$ and $\tilde{t}_2$ that are much lighter than all other $\tilde{f}$ and with $m_{\tilde{t}_1} \approx m_t$ are preferred, suggesting searches for supersymmetry through top quarks.

Assuming that $\tilde{t}_1$ is the next-to-lightest and $\tilde{\chi}_1^0$ is the lightest supersymmetric particle and thus is stable, three phase space regions with distinct decay modes can be identified as:

(i) $m_{\tilde{t}_1} - m_{\tilde{\chi}_1^0} > m_t$ with $\tilde{t}_1 \to t\tilde{\chi}_1^0$;

(ii) $m_W + m_b < m_{\tilde{t}_1} - m_{\tilde{\chi}_1^0} < m_t$ with $\tilde{t}_1 \to Wb\tilde{\chi}_1^0$;

(iii) $m_{\tilde{t}_1} - m_{\tilde{\chi}_1^0} < m_W + m_b$ with $\tilde{t}_1 \to W^*b\tilde{\chi}_1^0$ and W^* is an off-shell W boson, or $\tilde{t}_1 \to c\tilde{\chi}_1^0$ via loop-suppressed diagrams.

Many searches for supersymmetry at the Tevatron focused on the extended Higgs sector, which in many supersymmetric scenarios corresponds to that of 2HDM models summarised in Section 9.2. Beyond this, CDF searched for pair-produced stops in $\tilde{t}_1 \to b\tilde{\chi}_1^{\pm} \to W^{(*)}b\tilde{\chi}_1^0$ decay modes [204].

Decays in all three $m_{\tilde{t}_1}, m_{\tilde{\chi}_1^0}$ regions (i)–(iii) were explored to search for supersymmetry by ATLAS and CMS. A summary of the exclusion at 95% CL bounds by ATLAS using up to 20 fb^{-1} of data at $\sqrt{s} = 8$ TeV and 4.7 fb^{-1} at $\sqrt{s} = 7$ TeV is shown in Fig. 25. A substantial part of the $(m_{\tilde{t}_1}, m_{\tilde{\chi}_1^0})$ plane is experimentally excluded, and the different decay modes are covered by complementary analyses

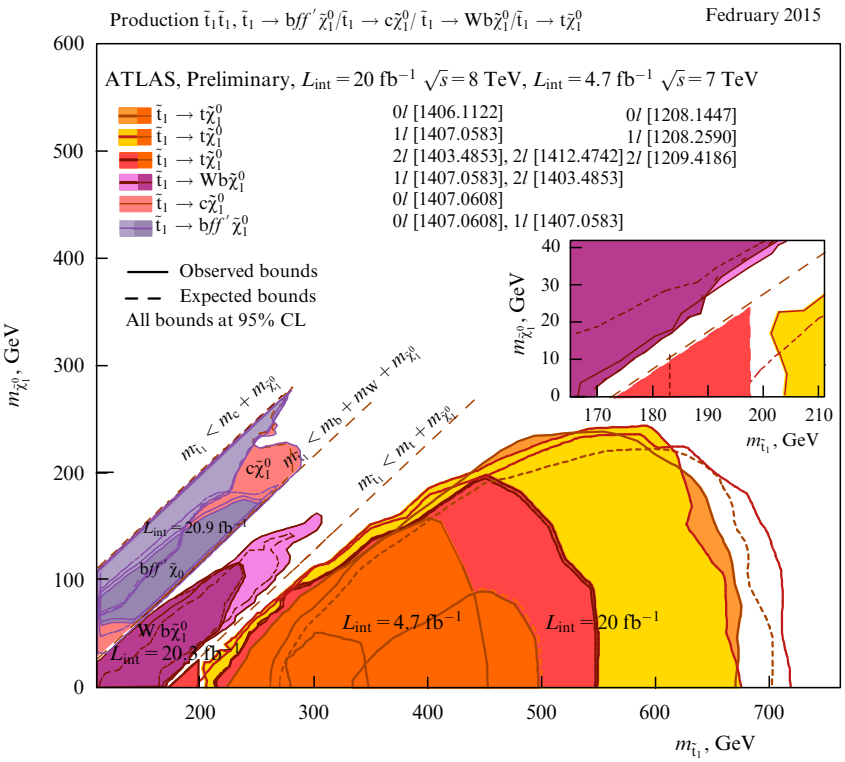

Figure 25. Overview of the ATLAS search results [205] for direct stop pair production for scenarios where no other supersymmetric particles besides $\tilde{t}_1$ and $\tilde{\chi}_1^0$ are involved in the $\tilde{t}_1$ decays. Observed (expected) exclusion bounds at a 95% CL are shown as solid (dashed) lines in the $m_{\tilde{t}_1} - m_{\tilde{\chi}_1^0}$ plane. The diagonal dashed straight lines indicate the three kinematic regimes (i)–(iii) discussed in the text, where different decay modes are considered with Br = 100.

reviewed in Ref. [205]. The exclusion sensitivity at high $m_{\tilde{t}_1}$ is driven by analyses exploiting boosted topologies and jet substructure techniques in the l+jets and all-jets channels. It extends to $m_{\tilde{t}_1} \approx 700$ GeV and is constrained by the size of the $t\bar{t}$ cross section in both channels. The intermediate kinematic regions at constant $m_{\tilde{t}_1} - m_{\tilde{\chi}_1^0}$ indicated by the dashed lines in Fig. 25 are experimentally challenging due to the similarity of the resulting signatures to those from SM processes. These regions are addressed by precision measurements of $\sigma_{t\bar{t}}$ in the eμ channel at $\sqrt{s} = 7$ TeV and $\sqrt{s} = 8$ TeV with an experimental uncertainty of about 4% [124], and by a measurement of the correlations between the spins of the t- and $\bar{t}$-quarks [206]. The exclusion bounds obtained by CMS are similar to those shown in Fig. 25, and come from Refs [207–211].

An alternative strategy employed by both ATLAS and CMS Collaborations is to search for the heavier stop mass eigenstate $\tilde{t}_2$, which then decays to $\tilde{t}_1$ [212, 213]. In the absence of a signal, exclusion bounds were set in the $(m_{\tilde{t}_1}\ m_{\tilde{t}_2})$ plane up to (450 GeV, 600 GeV). In addition, a $\tilde{t}_1$ signal was sought in pair production of gluinos ($\tilde{g}$), the superpartners of the gluons, by both ATLAS and CMS [214, 215], and exclusion bounds were set in the $(m_{\tilde{t}_1}, m_{\tilde{g}})$ plane up to (700 GeV, 1400 GeV).

9.4 Searches for vector-like quarks

Vector-like quarks (VLQs) have been proposed in many BSM scenarios, such as composite Higgs [216–218] and little Higgs models [219–222], mainly motivated to address the naturalness problem. VLQs are defined as quarks with left- and right-handed components transforming identically under $SU(2)_L$. Models with weak isospin singlets, doublets, and triplets have been proposed, where in the doublet case VLQs can occur as up quarks (T) or down quarks (B). VLQs predominantly decay to third generation quarks and produce signatures either involving top quarks or resembling them. Typical discrimination variables are H_T, defined as the scalar sum of the transverse momenta of all jets and possibly leptons, and the mass of T, m_T, determined through a kinematic fit.

At the Tevatron, searches focus on pair-produced VLQs which decay as B → Wt or T → Wb. CDF searched for $T\bar{T}$ production in the l+jets channel using $\mathcal{L} = 5.6$ fb^{-1} of data, and excluded $M_T < 360$ eV at 95% CL [223]. The exclusion of $M_T < 285$ GeV from D0 using $\mathcal{L} = 5.3$ fb^{-1} of data [224] is weaker due to a 2.5σ excess in the μ+jets channel. CDF excluded $M_B < 370$ GeV searching for $B\bar{B}$ production using $\mathcal{L} = 4.8$ fb^{-1} of data [225].

Similar search strategies are employed at the LHC; however, the potential decay modes are extended to B → Wt, Zb or Hb and T → Wb, Zt or Ht and some searches target the production of single VLQs. In some cases, signatures with same-sign final state leptons were used. In addition, for VLQ masses above about 500 GeV, boosted signatures and jet-substructure techniques (cf. Section 9.5) were applied.

In the absence of a signal, $M_T < 750(900)$ GeV are excluded at 95% CL for Br(T → Ht) = 1 (Br(T → Ht) = 0) by ATLAS [226–228], and $M_T < 650(800)$ GeV by CMS [229–233]. Similarly, $M_B < 600(800)$ GeV are excluded at a 95% CL for Br(B → Hb) = 1 (Br(B → Hb) = 0) by ATLAS [226–228, 234], and $M_B < 550(750)$ GeV by CMS [229, 230].

9.5 Searches for new gauge bosons

An extended gauge sector with massive gauge bosons, generically denoted as W′ or Z′, is predicted in many BSM scenarios, such as the Arkani-Hamed, Dimopoulos, Dvali

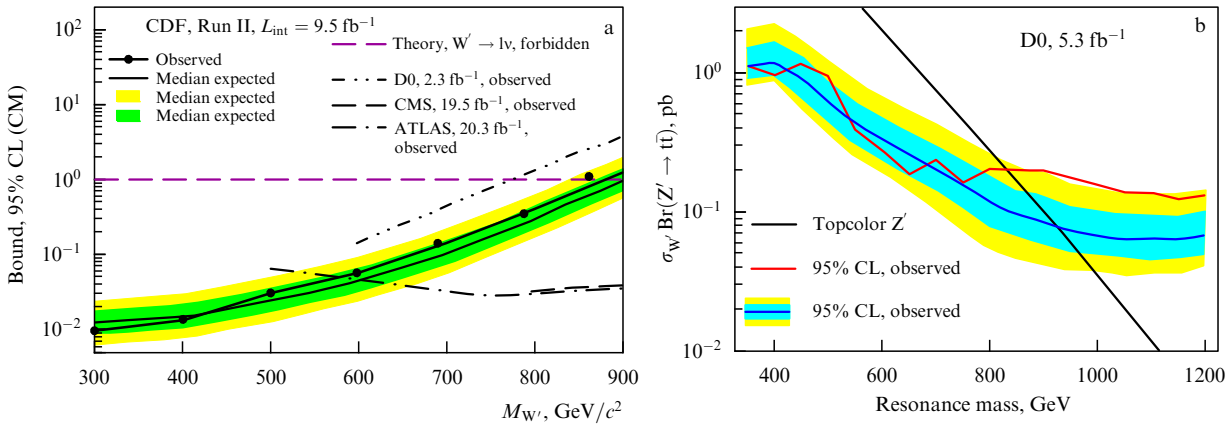

Figure 26. (Color online.) (a) Observed and expected upper bounds on $\sigma_{W'}\,\mathrm{Br}(W' \to t\bar{b})$ [239] at a 95% CL are compared to theory predictions for a right-handed W′-boson with SM-like coupling strengths. The exclusion bounds by D0 [238], ATLAS [240], and CMS [241] are also shown. (b) Observed and expected upper bounds on $\sigma_{Z'}\,\mathrm{Br}(Z' \to t\bar{t})$ of a narrow topcolor Z′ resonance [243] at a 95% CL are compared to theory predictions as a function of $M_{Z'}$. The shaded regions around the expected bound represent the 1σ and 2σ belts in figures (a) and (b).

model with large extra dimensions [235] or the Randall–Sundrum model with warped extra dimensions [236, 237], and many others.

Assuming that the W′ has SM-like V−A couplings, searches for $W' \to l\nu$ provide the best sensitivity. However, if the W′ couples only to right-handed particles and if hypothetical right-handed neutrinos are more massive than the W′, $W' \to t\bar{b}$ becomes the preferred search channel. Searches have also been performed for a leptophobic W′ boson with left-handed couplings. Typically, search strategies concentrate on single top-like $t\bar{b}$ production through the s-channel, and use the invariant mass distribution of the $t\bar{b}$ system as a discriminant. The first search for W′ with arbitrary couplings was conducted by D0 using $\mathcal{L} = 2.3$ fb^{-1} of data [238], and excluded $M_{W'} < 800$ GeV with purely left- or right-handed couplings. CDF excluded $M_{W'} < 900$ GeV with purely right-handed couplings using $\mathcal{L} = 9.5$ fb^{-1} of data as shown in Fig. 26a, and providing the world's most stringent bounds on W′ with $M_{W'} < 600$ GeV to date [239]. Similar search strategies were applied by the ATLAS and CMS Collaborations to $\mathcal{L} = 20.3$ fb^{-1} and $\mathcal{L} = 19.5$ fb^{-1} of data, resulting in observed (expected) exclusion bounds of $M_{W'} < 1.92$ TeV (1.75 TeV) [240] and $M_{W'} < 2.05$ TeV (2.02 TeV) [241], respectively, for a W′-boson with purely right-handed couplings.

Searches for $Z' \to t\bar{t}$ decays were conducted following the classical bump-hunt strategy in the invariant mass spectrum of the $t\bar{t}$ system for two generic scenarios: a resonance that is narrow relative to the detector resolution $\Gamma_{Z'}/m_{Z'} \approx 1\%$, representative of models such as topcolor [242], and a broad resonance $\Gamma_{Z'}/m_{Z'} = 10\,\% - 15\,\%$ as found, for example, in the Randall–Sundrum model with warped extra dimensions. In 2012, the search for Z′ resonances using $\mathcal{L} = 5.3$ fb^{-1} of data [243] by D0 sparked some interest with an excess of 2σ at $m_{t\bar{t}} \approx 1$ TeV, as shown in Fig. 26b, resulting in a much weaker observed bound of $m_{Z'} > 835$ GeV than the expectation of 920 GeV for narrow resonances. This excess was not confirmed by CDF, which excluded narrow Z′-bosons up to an observed (expected) bound of $m_{Z'} > 915(940)$ GeV using $\mathcal{L} = 9.5$ fb^{-1} of data. The sensitivity of such searches dramatically decreased beyond $m_{Z'} > 1$ TeV, because the three jets from the $t \to W^+(q'\bar{q})\,b$ decay can overlap in the (η, ϕ) plane and are not resolved as separate objects. This

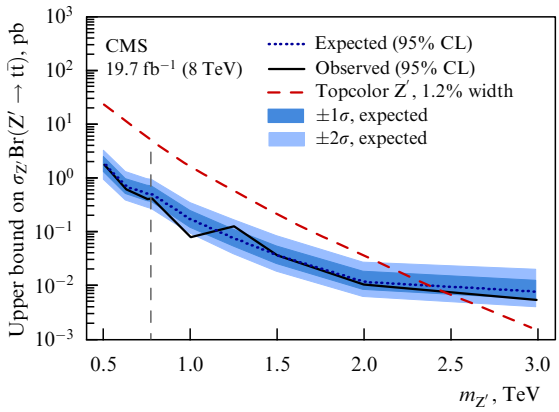

Figure 27. Observed and expected upper bounds on a narrow topcolor $Z' \to t\bar{t}$ resonance as a function of $M_{Z'}$ [246]. The shaded regions around the expected bound represent the $\pm1\sigma$ and $\pm2\sigma$ standard deviation belts. The predicted $\sigma_{Z'}\,\mathrm{Br}(Z' \to t\bar{t})$ is also given.

experimental challenge can be addressed by applying jet substructure techniques [244] to identify sub-jets resulting from the $t \to W^+(q'\bar{q})\,b$ decay products within wide jets.

ATLAS made a search for Z′ resonances using $\mathcal{L} = 20.3$ fb^{-1} of data and obtained observed (expected) exclusion bounds of $m_{Z'} > 1.8(2.0)$ TeV for narrow and of $m_{Z'} > 2.1(2.2)$ TeV for wide resonances in Randall–Sundrum scenarios [245]. The search by CMS using $\mathcal{L} = 19.7$ fb^{-1} of data found observed (expected) exclusion bounds of $m_{Z'} > 2.4(2.4)$ TeV for narrow resonances, as shown in Fig. 27, and of $m_{Z'} > 2.8(2.7)$ TeV for wide resonances in Randall–Sundrum models [247].

10. Conclusions

The top quark is strikingly different from other quarks and thus it plays a unique role in particle physics. It is the most massive of the quarks, and indeed of all SM particles. Because the Higgs Yukawa coupling is proportional to the fermion mass, the top quark Yukawa coupling is large — very close to unity. The large mass also makes the top-quark lifetime very much shorter than the time required to pull new quark–

antiquark states out of a vacuum and make hadrons. Therefore, uniquely, the top quark can be studied in its bare, unhadronized form. Despite the top quark's similarities to the other fermions in its basic quantum properties, it stands out as the exotic bird of paradise in the quark family portrait. Or is the top quark the model for what a quark should be, with the others as the odd sisters?

The virtual top-quark loops in the W-boson or Higgs boson propagators lead to very sensitive tests of the validity of the SM through the relationship of the masses of the top quark, the W-boson, and the Higgs boson. The measured top-quark mass is consistent with what is needed to drive the quartic coupling in the SM Higgs potential to negative values at large Q^2, leading to a possibly metastable universe. While the lifetime of the universe is extremely long, it is a puzzle that the top and Higgs masses should conspire so as to put the universe at the boundary between stability and instability.

In seeking new phenomena to explain the defects of the SM, most new models invoke large couplings between the new particles and the top quark, as seen in the very large Yukawa coupling of the Higgs boson to top quarks. Thus, we have the prospect of finding new particles such as heavy Z bosons or vector quarks whose decays contain top quarks, or particles such as charged Higgs bosons that could appear in the top decays. In supersymmetric models, the need for cancellation of the large loop contributions arising from the large top quark mass suggests that the companion top squarks should have a lower mass than other sparticle masses, thus making them prime candidates for a first sighting of supersymmetry. Despite the failure so far to find new physics in the production or decays of top quarks, the search remains highly motivated and will continue to be a dominant theme in the ongoing LHC program.

Although the top quark might seem to play no role in our everyday experience, its impact is nevertheless strong. If one assumes approximately unified $\mathrm{SU}(3) \times \mathrm{SU}(2) \times \mathrm{U}(1)$ couplings at a very high scale and allows them to evolve with decreasing Q^2, a break in the running α_s occurs at $Q = m_t$. If one continues to evolve to lower Q^2, one reaches the Λ_{QCD} scale, which, in turn, determines the proton mass. The resulting relation [247] $m_{\mathrm{proton}} \propto m_t^{2/27}$ implies that if the top-quark mass had the value originally expected of about $3 \times m_b$, the proton would weigh only 80% of what we observe, with dramatic consequences for our everyday world.

We expect the top quark to continue to be a portal for new discoveries.

Acknowledgments

We gratefully acknowledge support from the Federal Ministry of Education and Research (Germany); the Ministry of Education and Science of the Russian Federation, the National Research Centre 'Kurchatov Institute' of the Russian Federation, the Russian Foundation for Basic Research (Russia), and the Department of Energy and the National Science Foundation (United States). The work of one of us (E E B) was partially supported by the Ministry of Education and Science of the Russian Federation under grant No. NS-3042.2014.2.

References

1. Abe F et al. (CDF Collaboration) *Phys. Rev. Lett.* **74** 2626 (1995); hep-ex/9503002
2. Abachi S et al. (D0 Collaboration) *Phys. Rev. Lett.* **74** 2632 (1995); hep-ex/9503003
3. Gell-Mann M *Phys. Lett.* **8** 214 (1964)
4. Zweig G "An SU(3) model for strong interaction symmetry and its breaking", CERN-TH-412 (1964)
5. Aubert J et al. *Phys. Rev. Lett.* **33** 1404 (1974)
6. Augustin J-E et al. *Phys. Rev. Lett.* **33** 1406 (1974)
7. Glashow S L, Iliopoulos J, Maiani L *Phys. Rev. D* **2** 1285 (1970)
8. Perl M L et al. *Phys. Rev. Lett.* **35** 1489 (1975)
9. Herb S W et al. *Phys. Rev. Lett.* **39** 252 (1977)
10. ATLAS, CDF, CMS, D0 Collaborations "First combination of Tevatron and LHC measurements of the top-quark mass", arXiv:1403.4427
11. Cabibbo N *Phys. Rev. Lett.* **10** 531 (1963)
12. Kobayashi M, Maskawa T *Prog. Theor. Phys.* **49** 652 (1973)
13. Jeżabek M, Kühn J H *Phys. Rev. D* **48** R1910 (1993); *Phys. Rev. D* **49** 4970 (1994), erratum
14. Jeżabek M, Kühn J H *Nucl. Phys. B* **314** 1 (1989)
15. Bigi I I et al. *Phys. Lett. B* **181** 157 (1986)
16. Abbaneo D et al. (LEP Electroweak Working Group and SLD Heavy Flavor Group Collaborations) "A combination of preliminary electroweak measurements and constraints on the Standard Model", CERN-PPE-96-183, SLAC-REPRINT-1996-037
17. Baak M et al. *Eur. Phys. J. C* **74** 3046 (2014)
18. Branchina V, Messina E, Platania A *JHEP* (09) 182 (2014)
19. Weinberg S *Phys. Rev. Lett.* **19** 1264 (1967)
20. Salam A "Weak and electromagnetic interactions", in *Elementary Particle Theory. Proc. 8th Nobel Symp., 19–25 May 1968, Lerum, Sweden* (Ed. N Svartholm) (New York: Wiley; Stockholm: Almqvist and Wiksell, 1968) p. 367
21. Glashow S L *Nucl. Phys.* **22** 579 (1961)
22. Adeva B et al. (MARK-J Collaboration) *Phys. Rev. Lett.* **50** 799 (1983)
23. Behrend H J et al. (CELLO Collaboration) *Phys. Lett. B* **144** 297 (1984)
24. Altho M et al. (TASSO Collaboration) *Phys. Lett. B* **138** 441 (1984)
25. Abe K et al. (VENUS Collaboration) *Phys. Lett. B* **234** 382 (1990)
26. Abrams G S et al. (MARK II Collaboration) *Phys. Rev. Lett.* **63** 2447 (1989)
27. Decamp D et al. (ALEPH Collaboration) *Phys. Lett. B* **236** 511 (1990)
28. Abreu P et al. (DELPHI Collaboration) *Phys. Lett. B* **242** 536 (1990)
29. Akrawy M Z et al. (OPAL Collaboration) *Phys. Lett. B* **236** 364 (1990)
30. Arnison G et al. (UA1 Collaboration) *Phys. Lett. B* **147** 493 (1984)
31. Albajar C et al. (UA1 Collaboration) *Z. Phys. C* **37** 505 (1988)
32. Akesson T et al. (UA2 Collaboration) *Z. Phys. C* **46** 179 (1990)
33. Abe F et al. (CDF Collaboration) *Phys. Rev. Lett.* **68** 447 (1992)
34. Holmes S D, Shiltsev V *Annu. Rev. Nucl. Part. Sci* **63** 435 (2013)
35. Abachi S et al. (D0 Collaboration) *Phys. Rev. Lett.* **72** 2138 (1994)
36. Abe F et al. (CDF Collaboration) *Phys. Rev. D* **50** 2996 (1994)
37. Grannis P D, in *High Energy Physics. Proc. of the XXVII Intern. Conf., Glasgow, Scotland, 20–27 July 1994* (Eds P J Bussey, I G Knowles) (Bristol: Institute of Physics Publ., 1995) p. 15
38. Czakon M, Fiedler P, Mitov A *Phys. Rev. Lett.* **110** 252004 (2013)
39. Czakon M, Fiedler P, Mitov A *Phys. Rev. Lett.* **115** 052001 (2015)
40. Aaltonen T et al. (CDF, D0 Collaborations) *Phys. Rev. D* **89** 072001 (2014)
41. Abazov V M et al. (D0 Collaboration), D0 Note 6453-CONF (2015); *Phys. Rev. D*, to be submitted for publication
42. ATLAS, CMS Collaborations, ATLAS-CONF-2014-054, CMS-PAS-TOP-14-016 (2014)
43. Aaij R et al. (LHCb Collaboration) *Phys. Rev. Lett.* **115** 112001 (2015); arXiv:1506.0903
44. Abazov V M et al. (D0 Collaboration) *Phys. Rev. D* **90** 092006 (2014)
45. Aad G et al. (ATLAS Collaboration) *JHEP* (06) 100 (2015)
46. Rontsch R, Schulze M *JHEP* (07) 91 (2014)
47. Aad G et al. (ATLAS Collaboration) *Phys. Rev. D* **89** 072012 (2014)
48. Aad G et al. (ATLAS Collaboration), ATLAS-CONF-2012-126 (2012)

49. Chatrchyan S et al. (CMS Collaboration) *Phys. Rev. Lett.* **110** 172002 (2013)
50. Aad G et al. (ATLAS Collaboration), ATLAS-CONF-2014-038 (2014)
51. Chatrchyan S et al. (CMS Collaboration) *Eur. Phys. J. C* **74** 3060 (2014)
52. Chatrchyan S et al. (CMS Collaboration) *Phys. Lett. B* **746** 132 (2015)
53. Aad G et al. (ATLAS Collaboration), ATLAS-CONF-2012-130 (2012)
54. Aad G et al. (ATLAS Collaboration), ATLAS-CONF-2013-051 (2013)
55. Chatrchyan S et al. (CMS Collaboration) *JHEP* (11) 154 (2014)
56. Aaltonen T et al. (CDF Collaboration) *Phys. Rev. D* **83** 112003 (2011)
57. Abazov V M et al. (D0 Collaboration) *Phys. Rev. D* **84** 112005 (2011)
58. Aguilar-Saavedra J A et al. *Rev. Mod. Phys.* **87** 421 (2015)
59. Aaltonen T et al. (CDF Collaboration) *Phys. Rev. D* **87** 092002 (2013)
60. Abazov V M et al. (D0 Collaboration) *Phys. Rev. D* **90** 072011 (2014)
61. Abazov V M et al. (D0 Collaboration) *Phys. Rev. D* **92** 052007 (2015)
62. Aaltonen T et al. (CDF Collaboration) *Phys. Rev. Lett.* **113** 042001 (2014)
63. Abazov V M et al. (D0 Collaboration) *Phys. Rev. D* **90** 072001 (2014)
64. Bernreuther W, Si Z-G *Phys. Rev. D* **86** 034026 (2012)
65. Abazov V M et al. (D0 Collaboration) *Phys. Rev. D* **88** 112002 (2013)
66. Aad G et al. (ATLAS Collaboration) *JHEP* (02) 107 (2014)
67. Aad G et al. (ATLAS Collaboration) *JHEP* (05) 61 (2015)
68. Chatrchyan S et al. (CMS Collaboration) *Phys. Lett. B* **717** 129 (2012)
69. Chatrchyan S et al. (CMS Collaboration), CMS-PAS-TOP-12-033
70. Chatrchyan S et al. (CMS Collaboration) *JHEP* (04) 191 (2014)
71. Abazov V M et al. (D0 Collaboration) *Phys. Rev. Lett.* **108** 032004 (2012)
72. Bernreuther W et al. *Nucl. Phys. B* **690** 81 (2004)
73. Aaltonen T et al. (CDF Collaboration) *Phys. Rev. D* **83** 031104(R) (2011)
74. Aad G et al. (ATLAS Collaboration) *Phys. Rev. Lett.* **108** 212001 (2012)
75. Chatrchyan S et al. (CMS Collaboration) *Phys. Rev. Lett.* **112** 182001 (2014)
76. Aad G et al. (ATLAS Collaboration) *Phys. Rev. D* **90** 112016 (2014)
77. Abazov V M et al. (D0 Collaboration), D0 Note 6471-CONF (2015)
78. Aad G et al. (ATLAS Collaboration) *Phys. Rev. Lett.* **111** 232002 (2014)
79. Chatrchyan S et al. (CMS Collaboration), CMS-PAS-TOP-13-001 (2014)
80. Willenbrock S S D, Dicus D A *Phys. Rev. D* **34** 155 (1986)
81. Kidonakis N *Phys. Rev. D* **74** 114012 (2006)
82. Aaltonen T et al. (CDF Collaboration) *Phys. Rev. Lett.* **103** 092002 (2009)
83. Abazov V M et al. (D0 Collaboration) *Phys. Rev. Lett.* **103** 092001 (2009)
84. Breiman L et al. *Classification and Regression Trees* (Belmont, Calif.: Wadsworth Intern. Group, 1984)
85. Neal R M *Bayesian Learning for Neural Networks* (New York: Springer, 1996)
86. Boos E E et al. *Phys. Atom. Nucl.* **69** 1317 (2006); *Yad. Fiz.* **69** 1352 (2006)
87. Aaltonen T et al. (CDF, D0 Collaborations) *Phys. Rev. Lett.* **112** 231803 (2014)
88. Aaltonen T et al. (CDF, D0 Collaborations) *Phys. Rev. Lett.* **115** 152003 (2015)
89. Kidonakis N, in *Proc. of the XX Intern. Workshop on Deep-Inelastic Scattering and Related Subjects, Bonn, Germany, 2012*
90. Kidonakis N *Phys. Rev. D* **81** 054028 (2010)
91. Kidonakis N *Phys. Part. Nucl.* **45** 714 (2014); *Fiz. Elem. Chast. At. Yad.* **45** 1285 (2014)
92. Chatrchyan S et al. (CMS Collaboration) *Phys. Rev. Lett.* **112** 231802 (2014)
93. Neyman J, Pearson E S *Phil. Trans. R. Soc. Lond. A* **231** 289 (1933)
94. Aad G et al. (ATLAS Collaboration) *Eur. Phys. J. C* **75** 330 (2015)
95. Aad G et al. (ATLAS Collaboration), ATLAS-CONF-2014-055 (2014)
96. Aad G et al. (ATLAS Collaboration) *Eur. Phys. J. C* **75** 158 (2015)
97. Aaltonen T et al. (CDF Collaboration), CDF Note 11072 (2014)
98. Aaltonen T et al. (CDF Collaboration) *Phys. Rev. Lett.* **109** 152003 (2012)
99. Aaltonen T et al. (CDF Collaboration), CDF Note 11084 (2014)
100. Aaltonen T et al. (CDF Collaboration) *Phys. Rev. D* **88** 011101(R) (2013)
101. Chatrchyan S et al. (CMS Collaboration), CMS-PAS-TOP-14-014 (2014)
102. Chatrchyan S et al. (CMS Collaboration), CMS-PAS-TOP-14-001 (2014)
103. Chatrchyan S et al. (CMS Collaboration), CMS-PAS-TOP-14-002 (2014)
104. Abazov V M et al. (D0 Collaboration) *Phys. Lett. B* **752** 18 (2016)
105. Abazov V M et al. (D0 Collaboration) *Phys. Rev. Lett.* **113** 032002 (2014)
106. Bernreuther W, private communication (2012)
107. Olive K et al. (Particle Data Group) *Chin. Phys. C* **38** 090001 (2014)
108. Abazov V M et al. (D0 Collaboration) *Phys. Rev. D* **91** 112003 (2015)
109. Brandt O et al. *Nucl. Instrum. Meth. Phys. Res. A* **775** 27 (2015)
110. Abazov V M et al. (D0 Collaboration) *Phys. Rev. D* **84** 032004 (2011)
111. Lyons L, Gibaut D, Clifford P *Nucl. Instrum. Meth. Phys. Res. A* **270** 110 (1988)
112. Valassi A *Nucl. Instrum. Meth. Phys. Res. A* **500** 391 (2003)
113. Aaltonen T et al. (Tevatron Electroweak Working Group for CDF, D0 Collaborations), arXiv:1407.2682
114. Bigi I I et al. *Phys. Rev. D* **50** 2234 (1994)
115. Beneke M, Braun V M *Nucl. Phys. B* **426** 301 (1994)
116. Smith M C, Willenbrock S S *Phys. Rev. Lett.* **79** 3825 (1997)
117. Bardeen W A et al. *Phys. Rev. D* **18** 3998 (1978)
118. Fleming S et al., eConf C0705302 LOOP06 (2007)
119. Hoang A H, Stewart I W *Nucl. Phys. Proc. Suppl.* **185** 220 (2008)
120. Buckley A et al. *Phys. Rep.* **504** 145 (2011)
121. Aaltonen T et al. (CDF Collaboration) *Phys. Rev. Lett.* **100** 062005 (2008)
122. Abazov V M et al. (D0 Collaboration) *Phys. Rev. Lett.* **100** 192004 (2008)
123. Cacciari M et al. *JHEP* (04) 068 (2004)
124. Aad G et al. (ATLAS Collaboration) *Eur. Phys. J. C* **74** 3109 (2014)
125. Chatrchyan S et al. (CMS Collaboration) *Phys. Lett. B* **728** 496 (2014)
126. Alioli S et al. *Eur. Phys. J. C* **73** 2438 (2013)
127. Aad G et al. (ATLAS Collaboration), ATLAS-CONF-2014-053 (2014)
128. Gao J, Li C S, Zhu H X *Phys. Rev. Lett.* **110** 042001 (2013)
129. Aaltonen T et al. (CDF Collaboration), CDF Note 8104 (2005)
130. Aaltonen T et al. (CDF Collaboration) *Phys. Rev. Lett.* **111** 202001 (2013)
131. Abazov V M et al. (D0 Collaboration) *Phys. Rev. D* **85** 091104 (2012)
132. Abazov V M et al. (D0 Collaboration) *Phys. Lett. B* **705** 313 (2011)
133. Abazov V M et al. (D0 Collaboration) *Phys. Rev. Lett.* **107** 121802 (2011)
134. Chatrchyan S et al. (CMS Collaboration) *Phys. Lett. B* **736** 33 (2014)
135. Chatrchyan S et al. (CMS Collaboration) *JHEP* (12) 035 (2012)
136. Kidonakis N *Phys. Rev. D* **83** 091503(R) (2011)
137. Colladay D, Kostelecký V A *Phys. Rev. D* **55** 6760 (1997)
138. Greenberg O W *Phys. Rev. Lett.* **89** 231602 (2002)
139. Barenboim G, Lykken J *Phys. Lett. B* **554** 73 (2003)
140. Abazov V M et al. (D0 Collaboration) *Phys. Rev. D* **84** 052005 (2011)

141. Aaltonen T et al. (CDF Collaboration) *Phys. Rev. D* **87** 052013 (2013)
142. Chatrchyan S et al. (CMS Collaboration) *JHEP* (06) 109 (2012)
143. Aad G et al. (ATLAS Collaboration) *Phys. Lett. B* **728** 363 (2014)
144. Chang D, Chang W-F, Ma E *Phys. Rev. D* **59** 091503(R) (1999)
145. Chang D, Chang W-F, Ma E *Phys. Rev. D* **61** 037301 (2000)
146. Abazov V M et al. (D0 Collaboration) *Phys. Rev. Lett.* **98** 041801 (2007)
147. Abazov V M et al. (D0 Collaboration) *Phys. Rev. D* **90** 051101(R) (2014)
148. Aaltonen T et al. (CDF Collaboration) *Phys. Rev. D* **88** 032003 (2013)
149. Aad G et al. (ATLAS Collaboration) *JHEP* (11) 031 (2013)
150. Aaltonen T et al. (CDF Collaboration) *Phys. Rev. D* **82** 112005 (2010)
151. Abazov V M et al. (D0 Collaboration) *Phys. Rev. D* **84** 112001 (2011)
152. Kane G L, Ladinsky G A, Yuan C-P *Phys. Rev. D* **45** 124 (1992)
153. Czarnecki A, Korner J G, Piclum J H *Phys. Rev. D* **81** 111503 (2010)
154. Aaltonen T et al. (CDF, D0 Collaborations) *Phys. Rev. D* **85** 071106(R) (2012)
155. Aaltonen T et al. (CDF Collaboration) *Phys. Rev. D* **87** 031104(R) (2013)
156. Aad G et al. (ATLAS Collaboration) *JHEP* (06) 088 (2012)
157. Chatrchyan S et al. (CMS Collaboration) *JHEP* (01) 053 (2015)
158. Atwood D, Gupta S K, Soni A *JHEP* (06) 205 (2012)
159. Aaltonen T et al. (CDF Collaboration) *Phys. Rev. D* **87** 111101(R) (2013)
160. Aaltonen T et al. (CDF Collaboration) *Phys. Rev. Lett.* **112** 221801 (2014)
161. Higgs P W *Phys. Lett.* **12** 132 (1964)
162. Higgs P W *Phys. Rev. Lett.* **13** 508 (1964)
163. Higgs P W *Phys. Rev.* **145** 1156 (1966)
164. Englert F, Brout R *Phys. Rev. Lett.* **13** 321 (1964)
165. Guralnik G S, Hagen C R, Kibble T W B *Phys. Rev. Lett.* **13** 585 (1964)
166. Faddeev L D, Slavnov A A *Gauge Fields, Introduction to Quantum Theory* (Reading, Mass.: Addison-Wesley Publ. Co., 1991); Slavnov A A, Faddeev L D *Vvedenie v Kvantovuyu Teoriyu Kalibrovochnykh Polei* (Moscow: Nauka, 1988)
167. Peskin M E, Schroeder D V *An Introduction to Quantum Field Theory* (Reading, Mass.: Addison-Wesley Publ. Co., 1995)
168. Weinberg S *The Quantum Theory of Fields* Vols 1, 2 (Cambridge: Cambridge Univ. Press, 1995, 1996)
169. Bobeth C et al. *Phys. Rev. Lett.* **112** 101801 (2014)
170. Aaij R et al. (LHCb Collaboration) *Phys. Rev. Lett.* **111** 101805 (2013)
171. Chatrchyan S et al. (CMS Collaboration) *Phys. Rev. Lett.* **111** 101804 (2013)
172. Bezrukov F, Magnin A, Shaposhnikov M *Phys. Lett. B* **675** 88 (2009)
173. Bezrukov F et al. *JHEP* (10) 140 (2012)
174. Degrassi G et al. *JHEP* (08) 098 (2012)
175. Buttazzo D et al. *JHEP* (12) 089 (2013)
176. Bezrukov F, Shaposhnikov M *JETP* **120** 335 (2015); *Zh. Eksp. Teor. Fiz.* **147** 389 (2015)
177. Bezrukov F, Shaposhnikov M *Phys. Lett. B* **659** 703 (2008)
178. Bezrukov F, Rubio J, Shaposhnikov M *Phys. Rev. D* **92** 083512 (2015)
179. Branchina V, Messina E, Platania A *JHEP* (09) 182 (2014)
180. Witten E *Nucl. Phys. B* **188** 513 (1981)
181. Witten E *Nucl. Phys. B* **202** 253 (1982)
182. Sakai N *Z. Phys. C* **11** 153 (1981)
183. Dimopoulos S, Georgi H *Nucl. Phys. B* **193** 150 (1981)
184. Schael S et al. (ALEPH, DELPHI, L3, OPAL, LEP Electroweak Collaborations) *Phys. Rep.* **532** 119 (2013); The LEP Electroweak Working Group, http://lepewwg.web.cern.ch/LEPEWWG
185. Aad G et al. (ATLAS Collaboration) *Phys. Lett. B* **716** 1 (2012)
186. Chatrchyan S et al. (CMS Collaboration) *Phys. Lett. B* **716** 30 (2012)
187. Abazov V M et al. (D0 Collaboration), D0 Note 5739-CONF (2009)
188. Aaltonen T et al. (CDF Collaboration), CDF Note 10801 (2012)
189. Aad G et al. (ATLAS Collaboration) *Eur. Phys. J. C* **75** 349 (2015)
190. Chatrchyan S et al. (CMS Collaboration) *Eur. Phys. J. C* **75** 251 (2015)
191. Lee T D *Phys. Rev. D* **8** 1226 (1973)
192. Abazov V M et al. (D0 Collaboration) *Phys. Rev. Lett.* **102** 191802 (2009)
193. Chatrchyan S et al. (CMS Collaboration), CMS-PAS-HIG-13-026 (2014)
194. Aaltonen T et al. (CDF Collaboration) *Phys. Rev. Lett.* **96** 042003 (2006)
195. Abazov V M et al. (D0 Collaboration) *Phys. Rev. D* **80** 051107 (2009)
196. Abazov V M et al. (D0 Collaboration) *Phys. Rev. D* **80** 071102 (2009)
197. Aad G et al. (ATLAS Collaboration) *JHEP* (03) 088 (2015)
198. Chatrchyan S et al. (CMS Collaboration), CMS-PAS-HIG-14-020 (2014)
199. Aaltonen T et al. (CDF Collaboration) *Phys. Rev. Lett.* **103** 101803 (2009)
200. Aad G et al. (ATLAS Collaboration) *Eur. Phys. J. C* **73** 2465 (2013)
201. Chatrchyan S et al. (CMS Collaboration), CMS-PAS-HIG-13-035 (2014)
202. Abazov V M et al. (D0 Collaboration) *Phys. Lett. B* **682** 278 (2009)
203. Martin S P, in *Perspectives on Supersymmetry* (Advanced Series on Directions in High Energy Physics, Vol. 18, Ed. G L Kane) (Singapore: World Scientific, 1998) p. 1; hep-ph/9709356
204. Aaltonen T et al. (CDF Collaboration) *Phys. Rev. Lett.* **104** 251801 (2010)
205. Aad G et al. (ATLAS Collaboration) *Eur. Phys. J. C* **75** 510 (2015); arXiv:1506.08616
206. Aad G et al. (ATLAS Collaboration) *Phys. Rev. Lett.* **114** 142001 (2015)
207. Chatrchyan S et al. (CMS Collaboration) *Eur. Phys. J. C* **73** 2677 (2013)
208. Chatrchyan S et al. (CMS Collaboration), CMS-PAS-SUS-14-011 (2014)
209. Chatrchyan S et al. (CMS Collaboration), CMS-PAS-SUS-13-009 (2014)
210. Chatrchyan S et al. (CMS Collaboration), CMS-PAS-SUS-13-015 (2013)
211. Khachatryan V et al. (CMS Collaboration) *JHEP* (06) 116 (2015)
212. Aad G et al. (ATLAS Collaboration) *Eur. Phys. J. C* **74** 2883 (2014)
213. Khachatryan V et al. (CMS Collaboration) *Phys. Lett. B* **736** 371 (2014)
214. Aad G et al. (ATLAS Collaboration) *JHEP* (10) 024 (2014)
215. Chatrchyan S et al. (CMS Collaboration) *Phys. Lett. B* **733** 328 (2014)
216. Kaplan D B, Georgi H *Phys. Lett. B* **136** 183 (1984)
217. Kaplan D B, Georgi H, Dimopoulos S *Phys. Lett. B* **136** 187 (1984)
218. Georgi H, Kaplan D B *Phys. Lett. B* **145** 216 (1984)
219. Weinberg S *Phys. Rev. Lett.* **29** 1698 (1972)
220. Georgi H, Pais A *Phys. Rev. D* **10** 539 (1974)
221. Georgi H, Pais A *Phys. Rev. D* **12** 508 (1975)
222. Arkani-Hamed N, Cohen A G, Georgi H *Phys. Lett. B* **513** 232 (2001)
223. Aaltonen T et al. (CDF Collaboration) *Phys. Rev. Lett.* **107** 261801 (2011)
224. Abazov V M et al. (D0 Collaboration) *Phys. Rev. Lett.* **107** 082001 (2011)
225. Aaltonen T et al. (CDF Collaboration) *Phys. Rev. Lett.* **106** 141803 (2011)
226. Aad G et al. (ATLAS Collaboration), ATLAS-CONF-2015-012 (2015)
227. Aad G et al. (ATLAS Collaboration) *JHEP* (10) 150 (2015)
228. Aad G et al. (ATLAS Collaboration) *JHEP* (11) 104 (2014)
229. Khachatryan V et al. (CMS Collaboration) *Phys. Lett. B* **729** 149 (2014)
230. Chatrchyan S et al. (CMS Collaboration), CMS-PAS-B2G-12-019 (2013)
231. Khachatryan V et al. (CMS Collaboration), CMS-PAS-B2G-12-017 (2014)

232. Khachatryan V et al. (CMS Collaboration) *JHEP* (06) 080 (2015)
233. Khachatryan V et al. (CMS Collaboration), CMS-PAS-B2G-14-003 (2014)
234. Aad G et al. (ATLAS Collaboration) *Phys. Rev. D* **91** 112011 (2015)
235. Arkani-Hamed N, Dimopoulos S, Dvali G R *Phys. Lett. B* **429** 263 (1998)
236. Randall L, Sundrum R *Phys. Rev. Lett.* **83** 3370 (1999)
237. Randall L, Sundrum R *Phys. Rev. Lett.* **83** 4690 (1999)
238. Abazov V M et al. (D0 Collaboration) *Phys. Lett. B* **699** 145 (2011)
239. Aaltonen T et al. (CDF Collaboration) *Phys. Rev. Lett.* **115** 061801 (2015)
240. Aad G et al. (ATLAS Collaboration) *Phys. Lett. B* **743** 235 (2015)
241. Chatrchyan S et al. (CMS Collaboration) *JHEP* (05) 108 (2014)
242. Harris R M, Hill C T, Parke S J, hep-ph/9911288
243. Abazov V M et al. (D0 Collaboration) *Phys. Rev. D* **85** 051101(R) (2012)
244. Butterworth J M et al. *Phys. Rev. Lett.* **100** 242001 (2008)
245. Aad G et al. (ATLAS Collaboration) *JHEP* (08) 148 (2015); arXiv:1505.07018
246. Khachatryan V et al. (CMS Collaboration) *Phys. Rev. D* **93** 012001 (2016)
247. Quigg C, in *Proc. of the LAFEX Intern. School of High Energy Physics, Workshop on Heavy Flavors, cbt, Rio de Janeiro, February 1995*; hep-ph/9507257